

December 2017

Effects of Electrolyte Formulation on Graphite Anode for Wide Temperature Application

Jeremy Chang

University of Wisconsin-Milwaukee

Follow this and additional works at: <https://dc.uwm.edu/etd>



Part of the [Materials Science and Engineering Commons](#)

Recommended Citation

Chang, Jeremy, "Effects of Electrolyte Formulation on Graphite Anode for Wide Temperature Application" (2017). *Theses and Dissertations*. 1594.

<https://dc.uwm.edu/etd/1594>

This Thesis is brought to you for free and open access by UWM Digital Commons. It has been accepted for inclusion in Theses and Dissertations by an authorized administrator of UWM Digital Commons. For more information, please contact open-access@uwm.edu.

**EFFECTS OF ELECTROLYTE FORMULATION ON
GRAPHITE ANODE FOR WIDE TEMPERATURE
APPLICATION**

by

Jeremy Chang

A Thesis Submitted in
Partial Fulfillment of the
Requirements for the Degree of

Master of Science
in Engineering

at

The University of Wisconsin-Milwaukee

December 2017

ABSTRACT

EFFECTS OF ELECTROLYTE FORMULATION ON GRAPHITE ANODE FOR WIDE TEMPERATURE APPLICATION

by

Jeremy Chang

The University of Wisconsin-Milwaukee, 2017
Under the Supervision of Professor Benjamin Church

In this study, we demonstrate that the low temperature power capability of a Li-ion battery can be substantially improved not by adding exotic additives into the electrolyte, but by rational design of the composition of the most commonly used solvents. Through the detailed analysis with electrochemical impedance spectroscopy, the formation of a homogenous solid electrolyte interphase (SEI) layer on the carbon anode surface is critical to ensure the performance of a Li-ion battery in a wide temperature range. Subsequent post mortem analysis after cycling of the negative electrode by XPS revealed that all the electrolyte compositions form similar compounds in the solid electrolyte interphase. However, the higher capacity low temperature solvents showed a higher percentage of LiF and a lower percentage of carbon containing species such as lithium carbonate and lithium ethylene di-carbonate. The electrolyte composition where cyclic carbonates make up less than 25 % of the total solvent showed increased low temperature performance. Additionally, solvent composition with higher percentage of linear short chain carbonates also showed an improvement in low temperature performance. Lastly, there was no significant impact seen with high temperature performances in nearly all the combinations investigated.

TABLE OF CONTENTS

| | |
|--|------|
| ABSTRACT..... | ii |
| TABLE OF CONTENTS..... | iii |
| LIST OF FIGURES | v |
| LIST OF TABLES..... | vii |
| LIST OF SYMBOLS | viii |
| LIST OF ABBREVIATIONS..... | x |
| ACKNOWLEDGEMENTS..... | xii |
| CHAPTER 1 – INTRODUCTION | 1 |
| 1.1 Background..... | 1 |
| 1.2 Fundamentals of Battery Operation..... | 3 |
| 1.3 Start of Lithium-ion Technology | 7 |
| 1.4 Lithium-ion Electrolytes | 10 |
| 1.4.1 Salts..... | 11 |
| 1.4.2 Solvents..... | 13 |
| 1.5 Mechanism of SEI Formation..... | 17 |
| 1.6 Thermodynamics of Electrolytes | 19 |
| 1.7 Electrolyte Additives | 22 |
| 1.8 Remarks on Current State of Lithium-ion Electrolytes | 28 |
| CHAPTER 2 – METHODOLOGY | 30 |
| 2.1 Sample Preparation | 30 |
| 2.1.1 Coin Cell Fabrication..... | 30 |
| 2.1.2 XPS Specimens..... | 33 |
| 2.1.3 XRD Specimens..... | 33 |
| 2.2 Characterization Techniques..... | 34 |
| 2.2.1 Electrical performance testing | 34 |
| 2.2.2 X-ray Photoelectron Spectroscopy (XPS) | 39 |
| 2.2.3 X-ray Diffraction (XRD) | 41 |
| CHAPTER 3 – RESULTS AND DISCUSSION..... | 43 |
| 3.1 Electrical performance tests..... | 43 |
| 3.2 X-ray Photoelectron Spectroscopy (XPS) | 54 |
| 3.3 Electrochemical Impedance | 59 |
| 3.4 X-ray Diffraction (XRD) | 66 |
| CHAPTER 4 – ANALYSIS AND DISCUSSION | 71 |
| 4.1 Conclusions..... | 71 |

| | |
|--|----|
| 4.2 Future Work | 72 |
| REFERENCES | 74 |
| APPENDICES | 79 |
| Appendix A. -20°C and -30°C discharge capacity for various electrolyte at 5C rate after 100 cycles at 60°C | 79 |
| Appendix B. Elemental concentration on anode for electrolytes with VC and LiBOB additive..... | 81 |
| Appendix C. Cell cycling for electrolyte DOE..... | 83 |

LIST OF FIGURES

| | |
|---|----|
| FIGURE 1. Power and energy by battery type | 2 |
| FIGURE 2. Discharge mechanism of a lithium-ion battery | 5 |
| FIGURE 3. Li ⁺ insertion in graphite..... | 8 |
| FIGURE 4. Initial cycle of Li/graphite cell. F denotes irreversible capacity associated with SEI formation, E the irreversible capacity associated with exfoliation, and I the reversible capacity from lithium intercalation into graphite..... | 9 |
| FIGURE 5. Decomposition of electrolyte solvents by PF ₅ | 12 |
| FIGURE 6. Hydrolysis of LiPF ₆ from moisture | 12 |
| FIGURE 7. Schematic of SEI formation based on Besenhard's model | 19 |
| FIGURE 8. Phase Diagram of EC-based electrolyte..... | 20 |
| FIGURE 9. Phase diagram of EMC-EC with different LiPF ₆ salt concentrations | 21 |
| FIGURE 10. XPS spectra of VC and VC-free additive in EC-based electrolyte | 23 |
| FIGURE 11. Profiles of Li/graphite half-cells containing various salts in PC-based electrolyte..... | 26 |
| FIGURE 12. XPS C1s spectra for graphitic anode cycled in LiPF ₆ and LiBOB based electrolytes | 27 |
| FIGURE 13. Formation cycles and condition step at room temperature. CCCV C/5 charge until 4.1V, held at 4.1V until I=C/20, then 1 minute rest, followed by C/5 discharge to 2.7V (2 cycles). Lastly, CCCV 1C charge until 4.1V, held at 4.1V until I=C/20, then 1 minute rest, followed by 1C discharge to 2.0V (3 cycles)..... | 36 |
| FIGURE 14. Representative room temperature cycling. CCCV 1C charge until 4.1V, held at 4.1V until I=C/20, then 1 minute rest, followed by 5C discharge to 2.0V..... | 37 |
| FIGURE 15. Representative -20°C and -30°C cycling. CCCV 1C charge until 4.1V, held at 4.1V until I=C/20, then 2 hour rest, followed by 5C discharge to 2.0V..... | 37 |
| FIGURE 16. Representative room temperature, -20°C, and -30°C Discharge. Cells were discharged at 5C rate to 2.0V..... | 38 |
| FIGURE 17. Representative 60°C cycling repeated for 100 cycles. CCCV 1C charge until 4.1V, held at 4.1V until I=C/20, then 10 minute rest, followed by 5C discharge to 2.7V..... | 39 |

| | |
|---|----|
| FIGURE 18. Discharge capacity of different electrolytes containing various amount of cyclic carbonates including DEC at -20°C. The rate of discharge is 5C..... | 47 |
| FIGURE 19. Discharge capacity of different electrolytes containing various amounts of short chain linear carbonates and EC at -20°C. The rate of discharge is 5C. | 48 |
| FIGURE 20. Cox response plot of discharge capacity for different electrolytes at -20°C. The rate of discharge is 5C..... | 48 |
| FIGURE 21. Discharge capacity of different electrolytes containing various amounts of cyclic carbonates at -20°C. The rate of discharge is 5C..... | 49 |
| FIGURE 22. Discharge capacity of different electrolytes containing various amounts of linear carbonates except DEC at -20°C. The rate of discharge is 5C. | 50 |
| FIGURE 23. Discharge capacity of different electrolytes containing various amounts of linear carbonates at -20°C. The rate of discharge is 5C..... | 50 |
| FIGURE 24. A) Discharge curves of the electrolyte 9 at 5C rate at room temperature, -20°C and -30°C after the formation is complete. The cells were cooled for 2 hours before being discharged; B) Discharge curves of the electrolyte 9 at 5C rate at -20°C and -30°C after 100 cycles at 60°C. The cells were cooled for 2 hours before being discharged. The capacity loss at -20°C and -30°C is about 9% and 50% respectively compared with the fresh cells. | 52 |
| FIGURE 25. C1s (left) and O1s (right) XPS spectra of anodes cycles for 200 cycles at 60°C. ... | 54 |
| FIGURE 26. F1s (left) and P2p (right) XPS spectra of anodes cycles for 200 cycles at 60°C. ... | 55 |
| FIGURE 27. F1s (left) and C1s (right) graphs of discharge capacity (5C rate) vs. elemental concentration at -30°C. | 57 |
| FIGURE 28. LiF (left), $\text{Li}_x\text{PO}_y\text{F}_z$ (right), and C-O (bottom) graphs of discharge capacity (5C rate) vs. elemental concentration at -30°C..... | 59 |
| FIGURE 29. ac-impedance and fitting for fresh cells (after formation) at 25°C. The insets show the equivalent circuit used in the fitting and the enlargement of high frequency portion of the impedance spectra. | 61 |
| FIGURE 30. ac-impedance and fitting for fresh cells (after formation) at -20°C. The inset shows the equivalent circuit used in the fitting..... | 62 |
| FIGURE 31. XRD spectra of different electrolyte compositions..... | 68 |
| FIGURE 32. Plane Identification of Fresh Anode (Cu) | 68 |
| FIGURE 33. Plane Identification of Fresh Anode (Graphite) | 69 |
| FIGURE 34. XRD spectra of Graphite at 2θ of $\sim 26^\circ$ for different electrolyte compositions | 70 |

LIST OF TABLES

| | |
|--|----|
| TABLE 1. Lithium Salts | 13 |
| TABLE 2. Electrolyte Solvents | 14 |
| TABLE 3. Reduction Potentials of Solvents and Additives | 25 |
| TABLE 4. Electrolyte bounds used for DOE | 31 |
| TABLE 5. 1.0M LiPF ₆ Electrolytes with solvent variations and 1% VC/0.5% LiBOB as additive..... | 32 |
| TABLE 6. XPS settings for anode analysis | 41 |
| TABLE 7. Representative low temperature performance for various electrolytes from DOE..... | 43 |
| TABLE 8. Additional low temperature performance for various electrolytes | 44 |
| TABLE 9. Remaining low temperature performance for various electrolytes from DOE | 45 |
| TABLE 10. Elemental concentration on anode for different electrolytes | 56 |
| TABLE 11. Elemental concentration on anode for electrolytes with VC and LiBOB additive...57 | 57 |
| TABLE 12. Equivalent fitting results for the impedance spectra shown in figure 29 and 30 | 64 |
| TABLE 13. Low temperature performance for the cells after thermo-cycle at 60°C for 100 cycles..... | 65 |
| TABLE 14. Relative Intensities of Fresh Anode (Cu)..... | 69 |
| TABLE 15. Relative Intensities of Fresh Anode (Graphite) | 69 |
| TABLE 16. Future work on electrolyte compositions..... | 73 |

LIST OF SYMBOLS

| | |
|----------------|-----------------------------------|
| Li..... | Lithium |
| C..... | Carbon |
| F..... | Fluorine |
| O..... | Oxygen |
| P..... | Phosphorus |
| V..... | Voltage |
| A..... | Ampere |
| %..... | Percent |
| °C..... | Celsius |
| C..... | Capacity |
| cm..... | Centimeter |
| Ah..... | Amp-hour |
| mAh..... | Milliamp Hour |
| mA..... | Milliampere |
| M..... | Molar |
| g..... | Gram |
| W..... | Watt |
| Wh..... | Watt-hour |
| Kg..... | Kilogram |
| L..... | Liter |
| t_e | Electron transference number |
| θ | Angle of incidence in Bragg's Law |

| | |
|---------------------|--|
| \AA | Angstrom |
| A | Peak area |
| s | Sensitivity factor for XPS |
| Mg | Magnesium |
| Cs | Caesium |
| Σ | Summation |
| eV | Binding energy |
| d | Interplanar distance in Bragg's Law |
| λ | Wavelength of incident wave in Bragg's Law |
| θ | Angle |
| C1s | Carbon species |
| F1s | Fluorine species |
| O1s | Oxygen species |
| P2p | Phosphorus species |
| R_s | Ohmic resistance |
| C_{pseudo} | Pseudo capacitance |
| R | Diffusion resistance across SEI |
| R_{cte} | Charge transfer resistance |

LIST OF ABBREVIATIONS

| | |
|---------------------------------------|---|
| SHE..... | Standard Hydrogen Electrode |
| Ni-Cd..... | Nickel Cadmium |
| Ni-MH..... | Nickel Metal Hydride |
| Li-ion | Lithium-ion |
| LIB..... | Lithium-ion battery |
| EV..... | Electric vehicle |
| HEV..... | Hybrid electric vehicle |
| PHEV..... | Plug-in hybrid-electric vehicle |
| Redox | reduction-oxidation |
| LiPF ₆ | Lithium hexafluorophosphate |
| LiBF ₄ | Lithium tetrafluoroborate |
| LiClO ₄ | Lithium perchlorate |
| LiCoO ₂ | Lithium cobalt oxide |
| CsPF ₆ | Caesium hexafluorophosphate |
| NMC..... | Lithium nickel manganese cobalt |
| SEI..... | Solid electrolyte interphase |
| LEDC..... | (CH ₂ COCO ₂ Li) ₂ |
| LEC..... | Lithium ethyl carbonate |
| Li ₂ CO ₃ | Lithium carbonate |
| CH ₃ Oli..... | Lithium Methoxide |
| Li ₂ O..... | Lithium oxide |
| LiF..... | Lithium fluoride |

| | |
|-----------------------|---------------------------------------|
| PF ₅ | Phosphorus pentafluoride |
| LiBOB..... | Lithium bis(oxalato)borate |
| EC..... | Ethylene carbonate |
| PC..... | Propylene carbonate |
| EMC..... | Ethyl methyl carbonate |
| DMC..... | Dimethyl carbonate |
| DEC..... | Diethyl carbonate |
| MP..... | Melting point |
| BP..... | Boiling point |
| FP..... | Flash point |
| ESU..... | Dielectric constant |
| GIC..... | Graphite intercalation compound |
| XRD..... | X-ray diffraction |
| VC..... | Vinylene carbonate |
| XPS..... | X-ray photoelectron spectroscopy |
| PVDF..... | Polyvinylidene fluoride |
| GC..... | Glassy carbon |
| CCCV..... | Constant current and constant voltage |
| AC..... | Alternating current |
| IR..... | Internal resistance |
| CPE..... | Constant phase element |
| DOE..... | Design of experiment |

ACKNOWLEDGEMENTS

This thesis was a long time in the making, and many people have helped me along the way. I wish to thank Professor Dr. Deyang Qu for providing the idea and framework on how to go about investigating this project. I would also like to thank Professor Dr. Benjamin Church for introducing me to this project as it well aligned with my desire to learn more about lithium-ion batteries. In addition, Dr. Church has guided me throughout my graduate studies and has been a great advisor. Lastly, I could not have done this project without the full support of Joshua Harris and Dr. Janak Kafle. As I work full-time, Joshua Harris and Dr. Janak Kafle was more than accommodating when meeting out of normal hours discussing project updates and provided guidance for nearly a year.

This research was fully supported by my employer, Johnson Controls Inc. (JCI). I'd like to thank them for supporting not only in my research, but throughout my graduate studies.

I would also like to thank Dr. Steve Hardcastle for allowing me to use the Advanced Analytical Facility and Dr. Afsaneh Moghadam for training me on the various equipment's needed for this study.

CHAPTER 1 – INTRODUCTION

1.1 BACKGROUND

Efforts for rechargeable lithium batteries started in the 1980s with lithium metal used as the anode. The reason lithium metal as anode was so attractive is due to lithium having the lowest negative electrochemical potential (-3.04V vs. SHE) as well as being the lightest element (density = 0.534 g/cm³), capable of delivering a theoretical capacity of 3860 mAh/g. The electronegative property translates to a high cell voltage when matched with certain cathodes. The weight of the metal results in it having high specific capacity. Lithium was found to be stable in a number of nonaqueous solvents despite its reactivity [4]. The stabilization was attributed to the formation of a passivation film on the lithium surface, which prevents it from having a sustained reaction with electrolytes [2]. The efforts to expand from primary lithium-based batteries in the 1960s and 1970s continued toward lithium chemistry being used in rechargeable technology. However, there were instabilities in terms of cycle life and safety, as cycling the battery produced dendrites causing electrical shorts, leading to thermal runaway and possible explosion. Dendrites, or needlelike lithium crystals, would grow on the anode upon recharge and during discharge, become electrically isolated from the substrate due to nonuniform dissolution rates at different sites of the dendrite. Since then, research has shifted to using lithium ions with intercalated lithium metal oxide as electrode material. In 1991, Sony commercialized the first lithium-ion battery, and today has become the most promising and fastest growing battery type on the market. Today's lithium-ion batteries are found in nearly all consumer electronics, and recently has been gaining in popularity in the automotive industry. Electric vehicles can help increase fuel-efficiency, lower greenhouse gas emissions and air

pollution, as well as reduce the dependence on oil with vulnerability to price volatility and supply disruption. However, lithium-ion in the automotive application still faces many hurdles as of today, including performance and safety, high cost, infrastructure, and driving range. The current cost of lithium-ion batteries for vehicle applications is four to eight times that of lead acid batteries and one to four times that of nickel metal hydride [1]. A comparison of other technologies can be seen in Figure 1 below, where it shows the traditional lead acid batteries have the lowest power density (W/kg) and energy density (Wh/kg). Nickel metal hydride (Ni-MH) and Li-ion type batteries. There are also other emerging technologies not displayed that have the potential to go beyond that of Li-ion technology, however, is still far too early in development.

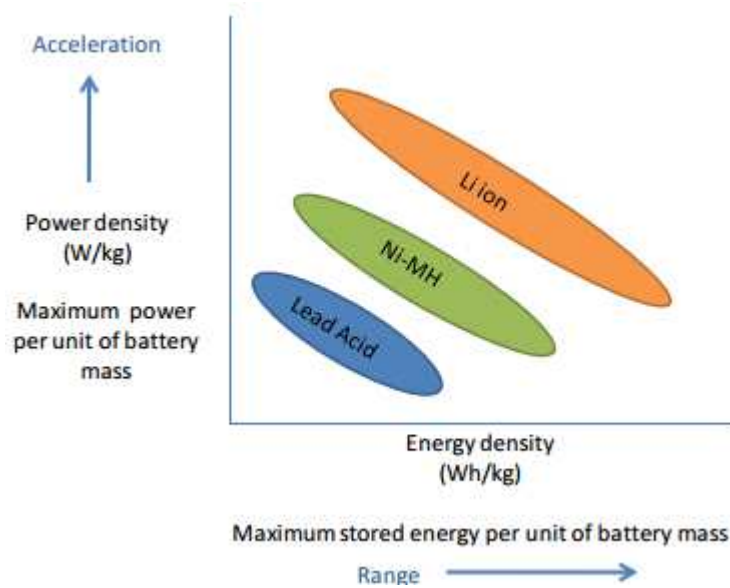


Figure 1. Power and energy by battery type [1]

The reemergence of electric vehicle demands have sparked new research for advancement in batteries. This newfound importance has come of late due to governmental requirements for increased fuel-efficiency, lower greenhouse gas emissions, and air pollution. Lithium-ion batteries (LIBs) have gained a lot of attention as one of the most promising power sources for

electric vehicles (EV), hybrid electric vehicles (HEV), and plug-in hybrid-electric vehicles (PHEV). It is estimated that by 2020, more than half of new vehicle sales will likely consist of hybrid-electric, plug-in hybrid, and all-electric models. While 96% of all hybrids available in the world today run on nickel metal hydride batteries, it is projected that 70% of hybrids, and 100% of plug-in hybrid and all-electric vehicles will run on lithium-ion batteries in the near future [1]. However, battery technology today are not able to meet the increasing demands of the consumers, leading to in-depth research in developing lithium-ion batteries with higher capacity and lower cost. Other stringent criteria's include high energy densities, moderate and consistent power densities, good safety, 10 year calendar-life, and a cycle-life of up to a few thousand charge and discharge cycles. Furthermore, current available LIBs for EVs are volatile, especially at high temperatures. Different studies have been made to improve the current issues including electrolyte development, alternative anode and cathode materials, and so forth. In this study, we will be focusing on electrolyte variations and its impact at low and high temperature extremes.

1.2 FUNDAMENTALS OF BATTERY OPERATION

A battery is a device that converts the chemical energy contained in its active material directly into electric energy by means of an electrochemical reduction-oxidation (redox) reaction [3]. For a rechargeable system, the battery is recharged by a reversal of this process. This involves transferring of electrons from one material to another through an electric circuit. Reaction in lithium-ion batteries involve three essential components. The positive electrode, negative electrode, and electrolyte. The positive electrode, or cathode, is the oxidizing electrode which accepts electrons from the external circuit and is reduced during discharge of a battery. The negative electrode, or anode, is the reducing electrode which gives up electrons to the external circuit and is oxidized during discharge of a battery. Lastly, the electrolyte, or ionic

conductor, provides the medium for transfer of charge, as ions, inside the cell between the anode and cathode [3]. Electrolytes used in lithium-ion batteries are typically a combination of lithium salts, such as LiPF_6 , LiBF_4 , or LiClO_4 , in an organic solvent.

During the operation of lithium-ion batteries, lithium ions move from the negative electrode to the positive electrode during discharge and vice versa when charging. A schematic of the operation of a cell is shown below in Figure 2 [1]. During discharge, electrons are released from the anode, becoming electric current, and travels to the outside circuit, then to the cathode. The anode becomes oxidized as electrons flow from the anode, and electrons are accepted by the cathode with the cathode material being reduced. During charge, the current flow is reversed and oxidation takes place at the positive electrode and reduction at the negative electrode. As the anode by definition is the electrode at which oxidation occurs and the cathode where reduction takes place, during charging the positive electrode is now the anode and the negative electrode the cathode. The chemical nature of the positive and negative electrodes dictate the energy output, whereas the electrolyte, in most situations, defines how fast the energy could be released by controlling the rate of mass flow within the battery [2]. As new electrode materials are coming into use, the need for compatible electrolytes also arises.

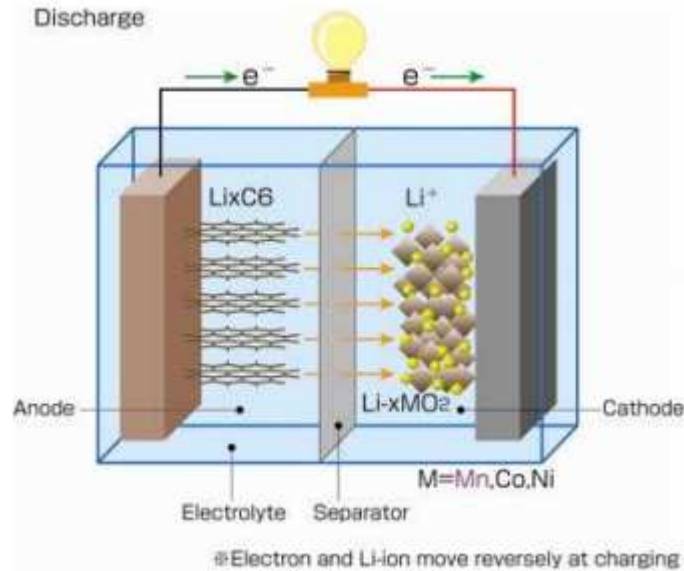


Figure 2. Discharge mechanism of a lithium-ion battery [1]

In a practical system, the components within the battery are selected based on the following properties. For anode, the efficiency as a reducing agent, high coulombic output (Ah/g), good conductivity, stability, ease of fabrication, and low cost. The cathode must be an efficient oxidizing agent, be stable when in contact with the electrolyte, and have a useful working voltage. Most common cathode materials in lithium-ion batteries are metallic oxides. Lastly, the electrolyte should have good ionic conductivity, nonreactive with electrode materials, minimal change with temperature fluctuations, safety in handling, and low cost. Separator materials are also used to separate the anode and cathode materials to prevent internal short-circuits. This material is permeable to allow the electrolyte to maintain its ionic conductivity.

Many different types of lithium-ion cathode materials have been developed such as LiCoO_2 , as it is the most commercially available material and has shown good electrical performance. However, due to its high cost of raw materials and safety issues, battery makers have opted for cheaper and safer alternatives. Among the attractive alternatives to LiCoO_2 for

cathode materials is the layered lithium-nickel-manganese-cobalt (NMC) oxide that have piqued interest since its introduction in early 2000s. NMC as a cathode material has relatively low cost, high capacity, and good thermal stability [51-52]. Additionally, NMC has a moderate high rate capability, lower solubility to solvents, smaller volume change and gas evolution during charge, and lower toxicity than other materials. Below is the half-cell reaction for a typical transition metal oxide used as positive electrode:



NMC cathode combination is typically one-third nickel, one-third manganese, and one-third cobalt, also known as 1-1-1. This unique blend takes advantage of the combination between nickel and manganese, as nickel is known for its high specific energy and manganese to achieve low internal resistance due to its stable spinel structure. NMC as cathode is used in this study as it is currently the leading contender for automotive applications in addition to the many advantages briefly described over conventional metal oxides.

Electrolytes serve as the medium for the transfer of charges, which are in the form of ions, between a pair of electrodes [2]. The majority of electrolytes in batteries consist of salts dissolved in solvents, either in water (aqueous) or organic solvents (nonaqueous). The electrolyte should not go through any net chemical changes during the operation of a battery, and all Faradaic processes are expected to occur within the electrodes. The electrolyte can be considered as an inert component of the battery and must have stability against both cathode and anode surfaces. The electrochemical stability of the electrolyte is usually realized in a kinetic (passivation) manner versus thermodynamic, but is often challenged by the strong oxidizing and reducing nature of the cathode and anode, respectively [2]. The increasing demand of new battery systems drive the research of more oxidizing cathode and more reducing anode as

electrode materials, thus constantly needing to make improvements in electrolyte stability. While the electrode materials can be quantified by the redox potential in volts against a reference potential, the stability of the electrolyte can be quantified by the range in volts between its oxidative and reductive decomposition limits [2]. Thus, the electrolyte should have a wide electrochemical window so that it doesn't degrade within the range of the working potentials between the electrodes. Not only should the electrolyte have good stability, but also should be a good ionic conductor and electronic insulator for ease of ion transport and self-discharge can be kept to a minimum. It should also be inert to other cell components, robust against abuses, and environmentally friendly.

1.3 START OF LITHIUM-ION TECHNOLOGY

As previously mentioned, the failure of lithium as an anode due to dendrite formation sparked research in ways to avoid the morphological change of the anode during cycling. As a result, intercalation type electrodes were considered, which had been applied earlier to cathode materials for lithium batteries, as done by Whittingham, Goodenough, and others [19-22]. These intercalation type electrodes were also considered as "host-guest" materials, with most being transition metal oxides having stable crystal lattices, allowing pathways for guest ions such as lithium ion to diffuse through their structures. Alternatively, research was also done by Japanese scientists that used materials containing carbon as anode intercalation hosts [9-11]. In the charged state of these new anodes, lithium exists in its ionic state rather than metallic state, therefore eliminating any possibility of lithium dendrites. In addition, the high lithium ion activity help the anode potential be close to that of lithium metal. Dahn et al. published their report on the principle of lithium intercalation chemistry with graphitic anodes and the effect of

electrolyte solvent in the process [12]. Figure 3 below shows how lithium is intercalated in between graphite planes of graphite from a side and top view, respectively.

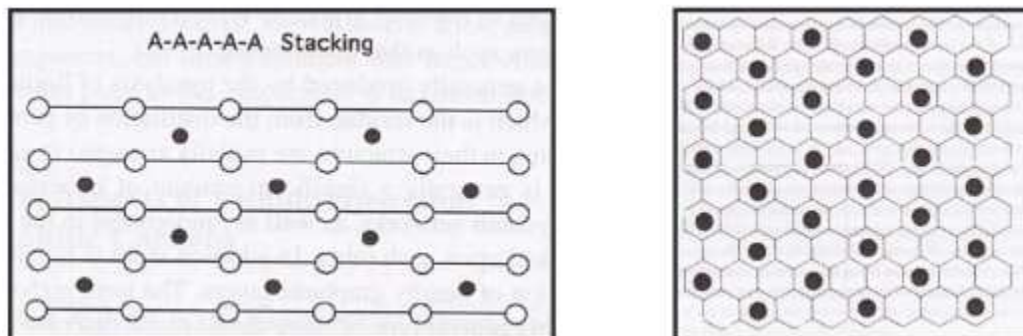
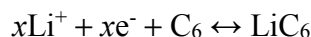


Figure 3. Li^+ insertion in graphite [3]

A negative electrode based on intercalated lithium in graphite would have the following half-cell reaction:



In their findings, electrolyte solvents reduce on the anode and decompose forming a protective film, which prevents further decomposition of the electrolyte components. This film was found to act as an ionic conductor but also electrically insulating. Furthermore, the reduction process occurs only during the first charge and is absent in the following cycles so that the anode can be cycled many times in the electrolyte. The chemical structure of the electrolyte solvents influence the nature of the protective film, and ethylene carbonate was found to be an essential component of the solvents that protects the crystalline structure of graphite. Dahn et al. named this surface film on carbonaceous anodes as “solid electrolyte interphase”, or SEI. The concept of the SEI layer was originally proposed by Peled in which a protective film was generated on the lithium anode when lithium metal was first found to be stable in nonaqueous electrolytes [31]. This term is used frequently in lithium-ion publications, however, its formation mechanism is still a topic

that's not clearly understood, even today. For graphitic anodes, Dahn accounted for the irreversible capacity around 1.2V which followed a linear relationship with the surface area of graphite anode and that this process is nonexistent in the following cycles. As seen in Figure 4, "F" portion shows the irreversible capacity that comes from SEI formation at 1.2V. Then at 0.8V represented by portion "E", the irreversible capacity stems from exfoliation of the graphite. Lastly, "I" portion shows the reversible capacity at very low potential, <0.20 V, to support lithium ion intercalation and deintercalation. Therefore, Dahn speculated that a passivation film similar to the one proposed by Peled was formed on graphite via a similar electrolyte decomposition. The SEI term that Peled had introduced for lithium anode was then also used for graphitic anode materials.

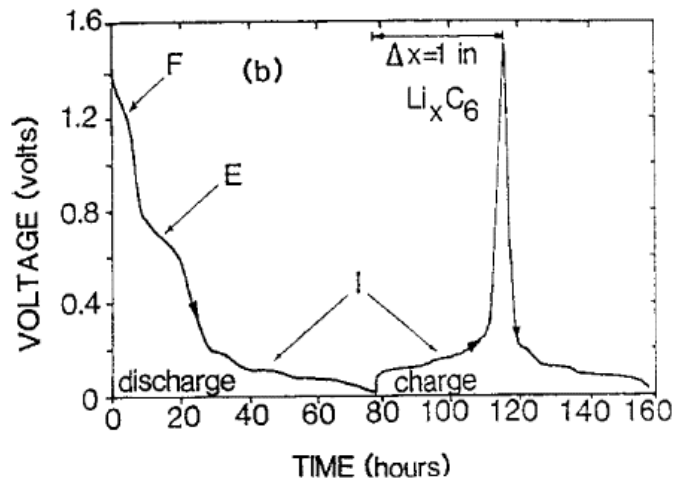


Figure 4. Initial cycle of Li/graphite cell. F denotes irreversible capacity associated with SEI formation, E the irreversible capacity associated with exfoliation, and I the reversible capacity from lithium intercalation into graphite. [12]

It is generally accepted that the SEI layer is mainly comprised of electrolyte reduction products and heavily influence the properties of the electrode. It has been reported that the composition of the anode SEI generated include a complex mixture of compounds such as LEDC

$(\text{CH}_2\text{COCO}_2\text{Li})_2$, LEC (lithium ethyl carbonate, $\text{CH}_3\text{CH}_2\text{OCO}_2\text{Li}$), Li_2CO_3 , CH_3OLi , $\text{CH}_3\text{CH}_2\text{OLi}$, $\text{LiOCH}_2\text{CH}_2\text{OLi}$, Li_2O , LiF , and $\text{Li}_x\text{PF}_y\text{O}_z$ [30]. Thus, it is believed that the chemical nature of the SEI is dictated by the electrolyte composition. However, many studies in proving the makeup of the SEI layer through different characterization methods has proven difficult, as it has structural similarities to the components of the electrolyte. The SEI layer ideally functions as a passivation layer and is lithium ion conducting but electrically insulating, allowing lithium ions to intercalate and deintercalate the electrode while preventing further electrolyte reduction at the anode surface [13]. The ideal SEI would constitute the following: (1) electron transference number $t_e = 0$, (2) high ionic conductivity in order for lithium ion to migrate to and from graphene layers, (3) uniform morphology and composition for current distribution, (4) good adhesion to anode, (5) good mechanical strength and flexibility to allow for expansion/contraction of graphene layers during intercalation/deintercalation of lithium ion, and (6) low solubility in electrolytes.

1.4 LITHIUM-ION ELECTROLYTES

As lithium-ion technology has seen a recent amount of tremendous growth, many researches have been focused on new materials for the anode and cathode, and not so much an emphasis on other cell components. This study is to better understand the effects of electrolyte, as this component interacts closely with both the cathode and anode during operation as well as heavily influencing the nature of the SEI. Many electrolytes used for lithium-ion are based on solutions of one or more lithium salts with at least two solvents. The reason for typically more than two solvents is the multiple requirement of the battery applications, which cannot usually be met with only one type. However, there is usually not a mixture of salts, as the choices are limited and performance advantages have yet to be proven.

1.4.1 LITHIUM-ION ELECTROLYTES - SALTS

One of the components involved in lithium-ion electrolytes are lithium salts. The basic requirements for an electrolyte solute include being able to dissolve and dissociate in nonaqueous solvent, solvated ions should have high mobility, the anion should be stable against oxidative decomposition at the cathode, and both cation and anion should remain inert toward other cell components. In the current state of lithium-ion technology, there are not many available options for lithium salts. Due to the small ionic radius of lithium ion, most salts of lithium do not meet the minimum solubility requirements. The lithium salts that do qualify for solubility are anions which are stabilized by a Lewis acid agent.

Of the limited options for lithium-ion batteries, lithium hexafluorophosphate (LiPF_6) is among the most widely known and used commercially. LiPF_6 was first proposed in the late 1960, but initially had a series of issues such as sensitivity toward moisture which made it difficult in the salts preparation for commercial use. Also, this solute was soon known to have chemical and thermal instabilities [28]. At elevated temperatures, the solute will produce LiF (s) and PF_5 (g) as shown:



Leading to a series of side reactions from PF_5 in the presence of nonaqueous solvents. Figure 5 below shows the decomposed product which results in ring-opening polymerizations of cyclic esters and cleavage of linear esters.

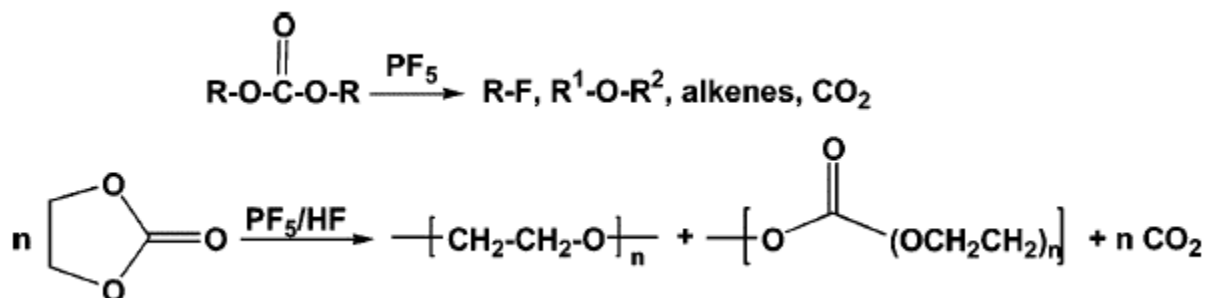


Figure 5. Decomposition of electrolyte solvents by PF₅ [2]

This solute also had issues with hydrolysis with even small amounts of moisture present. Figure 6 below shows the decomposition into corrosive products in the presence of moisture:

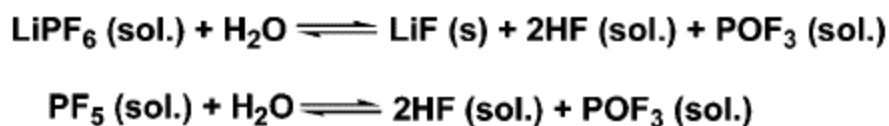
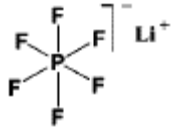
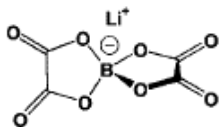


Figure 6. Hydrolysis of LiPF₆ from moisture [2]

However, by the late 1980s, manufacturers were able to obtain high-purity LiPF₆ through process improvements which finally lead to its commercialization and further research. LiPF₆ does not have a single outstanding property that makes it better than other available lithium salts, however, has the combined effect of multiple properties unachievable by other salts. Properties such as conductivity, dissociation constant, ionic mobility, thermal stability, anodic stability, and chemical stability are not exceptionally great for LiPF₆, though none of the other salts could meet all these requirements simultaneously. Table 1 below lists the basic physical properties of LiPF₆ that was used in this study. In addition, LiBOB is also included in this table as it was another salt that was studied. Further discussion on LiBOB salt will be discussed in the Section 1.7.

Table 1. Lithium Salts

| Salt | Structure | Molecular Wt. (g/mol) | M.P. (°C) |
|-------------------|---|-----------------------|-----------|
| LiPF ₆ |  | 151.91 | 200 |
| LiBOB |  | 193.9 | >300 |

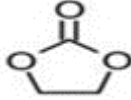
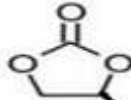
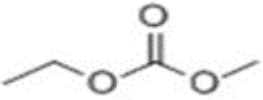
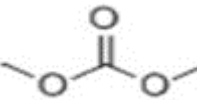
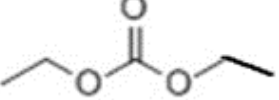
For nonaqueous solvents based on esters, LiPF₆ is one of the most conducting salts available. This is because LiPF₆ has both good ionic mobility and dissociation constant, although as previously mentioned, it is not the most outstanding in either category on its own. A typical nonaqueous electrolyte system consists of approximately 1.0 M lithium hexafluorophosphate (LiPF₆) dissolved in organic carbonate solvents. Studies have shown that LiPF₆ in mixed esters can also resist oxidation of up to 5.1V, making it one of the few salts that can support the operation of high voltage cathode material [23].

1.4.2 LITHIUM-ION ELECTROLYTES - SOLVENTS

The ideal solvent in lithium-ion electrolytes should be able to dissolve salts (ie. high dielectric constant), low viscosity, inert to cell components, and have no phase changes at various temperatures. The desire for low viscosity is to aid in ion transportation, which correlates to the need for solvent to be liquid at a wide temperature range. Nonaqueous compounds with polar groups are suited best as electrolyte solvents as they are able to dissolve sufficient amounts of lithium salt. Typical solvents have mainly been from organic esters and ethers in lithium-ion technology. The most commonly used solvent system is the mixture of

ethylene carbonate (EC) and ethyl methyl carbonate (EMC) in 3:7 ratio [53-55]. In this study, multiple solvents were investigated, including EC (ethylene carbonate), PC (propylene carbonate), EMC (ethyl methyl carbonate), DMC (dimethyl carbonate), and DEC (diethyl carbonate). Table 2 shows the difference between these solvents and their properties, including their molecular weight, melting point, boiling point, flash point, and dielectric constant. It can be assumed that by varying their ratios within an electrolyte mixture, cell performance can be altered. One noticeable difference that can be seen between the electrolyte solvents is that all the acyclic esters have a low dielectric constant, whereas cyclic esters have a relatively high dielectric constant. Cyclic esters has been commonly used as they exhibit a very wide electrochemical stability window and can effectively dissociate a large amount of lithium salts and hence provide high ionic conductivity.

Table 2. Electrolyte Solvents

| Solvent | Structure | Molecular Wt. (g/mol) | M.P. (°C) | B.P. (°C) | F.P. (°C) | Dielectric Constant (esu) |
|---------|---|-----------------------|-----------|-----------|-----------|---------------------------|
| EC |  | 88.06 | 35 | 243 | 143 | 89.6 |
| PC |  | 102.09 | -55 | 242 | 275 | 65 |
| EMC |  | 104.12 | -53 | 107.5 | 26.7 | 2.99 |
| DMC |  | 90.08 | 3 | 90 | 17 | 3.1 |
| DEC |  | 118.13 | -74 | 126 | 25 | 2.8 |

One such cyclic ester within this study is propylene carbonate, or PC for short. Interest grew for this solvent mainly due to its high dielectric constant and its ability to dissolve a wide variety of lithium salts. The high dielectric constant of 65 makes this solvent frequently used as a high-permittivity component when in conjunction with a low viscosity solvent. Its high polarity is also able to create an effective solvation shell around the lithium ions, which creates a conductive electrolyte. However, studies in the past have shown that electrolytes containing PC have poor cycling performances due to continuous electrolyte reduction from the lack of a stable anode SEI formation [14]. Reasons why PC solvents lead to poor cycling have attributed the shortcomings to cointercalation of PC solvent molecules with lithium cation into the graphite sheets, leading to exfoliation of the graphite [15-17]. This type of failure follows Besenhard's model of how an SEI layer is formed, which will be further discussed in the next section. PC solvents were also found to be reduced at potentials around 1.0 V (Li/Li⁺) forming ROCO₂Li and reversible intercalation of Li⁺ in graphite is not possible [13, 38]. Other studies have also attributed the poor performance to the physical properties of the electrolyte reduction products [18-20].

The other cyclic ester of interest in the lithium-ion industry is ethylene carbonate, or EC. In comparison with PC, EC has a slightly lower viscosity and higher dielectric constant at 89.6, which are all favorable attributes in selecting an electrolyte for lithium-ion batteries. Initially however, due to its high melting point, which is around 36°C, it was not a good candidate for ambient temperature electrolyte solvent, as its liquid range was too limited and could not be used alone. A study done in 1970 by Pistoia, De Rossi, and Scrosati showed the advantages of having EC as an electrolyte solvent. They were able to achieve liquid solutions at room temperature with EC in the presence of specific salts [21]. Additionally, it was reported that the specific

conductivities of the electrolyte solutions in EC are greater than those of the corresponding solutions in PC. Following this among other reports, EC was starting to be used in conjunction with PC as the electrolyte solvent. Through the work of Dahn et al., they were able to find a difference in EC and PC in regards to their effects on the reversibility of lithium ion intercalation and deintercalation with graphite anodes. EC was found to form an effective SEI layer on the anode that prevented any further electrolyte decomposition on the anode, whereas this was not achievable for PC.

Efforts in the 1990s focused on using EC based electrolytes with other possible cosolvents. None of the cosolvents investigated performed well however, due to PC causing irreversible capacity in the initial cycle, in addition to ethers being unstable against oxidation from the charged cathode. In 1994, Tarascon and Guyomard found a suitable electrolyte using EC based electrolyte with DMC (dimethyl carbonate) as a cosolvent [22-23]. Linear carbonates such as DMC have a low boiling point, low viscosity, and low dielectric constant. They are able to form homogenous mixtures with EC at any ratio, and the results of this mixed electrolyte lowered the melting-temperature of EC as well as having lower overall viscosity, resulting in higher ion conductivity. Additionally, the electrochemical stability of this mixture also did not change much, which came as a surprise, as linear carbonates are prone to oxidation on cathode surfaces. The resulting mixture between EC and DMC showed qualities of each individual solvent, where there was high anodic stability of EC on the cathode surface, high solvation ability of EC toward lithium salts, and low viscosity of DMC for ion transportation. The formulation between EC and a linear carbonate sparked researchers and manufacturers to explore different linear carbonates, including EMC and DEC. Aurbach et al. studied the effects of EMC electrolyte and showed that graphite electrodes in single-solvent EMC solutions perform well

versus pure DMC and diethyl carbonate (DEC). EMC-EC mixtures also performed just as well as pure EMC electrolyte. They attributed this performance improvement partially due to the surface films formed containing Li_2CO_3 , which is a very good passivating agent [44]. Aurbach also showed the effect of graphite electrodes in EC-DEC solutions which can be cycled at high capacity for hundreds of cycles due to the surface films on the electrodes [45].

Overall when these solvents are mixed, their physical properties change dramatically. For example, PC has a very low melting point, but its viscosity is comparably high. DMC is less viscous but has higher melting point (3°C). EMC has a low melting point (-53°C) and DEC has the lowest melting point (-74°C) among all the carbonates. The dielectric constant values of these solvents also vary widely; liquid EC (89.6 esu) and PC (65 esu) have very high values. The linear carbonates have low dielectric constants values (approximately 3 esu).

1.5 MECHANISM OF SEI FORMATION

As previously mentioned, many studies have found that the SEI layer is mainly comprised of electrolyte reduction products. Two principal models have been theorized and commonly adopted on how the SEI layer is formed, one being Peled's model which entails that the passivation film is established via a simple surface reaction, and the second being Besenhard's model, which involves ternary graphite intercalation compounds (GIC). According to Peled's model, the film is not expected to form until the potential of the anode is cathodically polarized, as the potentials of the anode is much higher than the reduction potentials of most solvents. In addition to this model, the SEI is formed by preferential reduction of certain electrolytes in a stepwise process. Endo et al. investigated the reductive decomposition of various electrolytes and found that the reduction of cyclic carbonates such as EC and PC were the main species comprising of the SEI while linear carbonate species were very minimal [32].

Additionally, in contrast to Besenhard's model, Aurbach interpreted graphite exfoliation as destruction of electrode structure at a macroscopic level, caused by gaseous products generated due to poor passivation properties from the initial SEI [38,46]. In contrast to Peled's proposal, Besenhard et al. suggested that the reductive decomposition of electrolytes was not by a simple surface reaction. It was argued that the solvent cointercalated into graphene layers, with the initial formation of a ternary GIC $[\text{Li}(\text{solvent})_x\text{C}_y]$, prior to their decomposition, and then the passivation layer formed could then penetrate into the graphene structure. Figure 7 below shows a schematic illustration of SEI formation mechanism proposed by Besenhard that has subsequent decomposition near the edge of graphene layers to form the SEI. Besenhard's evidence for this mechanism on the graphite electrode was supported through dilatometric measurements, which indicated a crystal expansion of 150% [33]. However, subsequent XRD measurements conducted by other researchers failed to confirm any significant changes in the distance between graphene layers during cointercalation. Additionally, the change in 2θ of the diffraction peak from these studies correspond to an expansion able to only accommodate lithium ions at 0.35\AA [36-38]. Other studies have defended Besenhard's model, stating that the lack of XRD evidence may be due to rapid decomposition or presence near graphite edges not being able to detect the ternary graphite intercalation compound. Despite concerns raised, the Besenhard model has received much support and has become the prevalent model used by researchers in the industry.

In summary, various models have been proposed to illustrate the formation of an SEI layer on graphite anode, based on the notion that the SEI is comprised mainly of reduced electrolyte components. The main difference between the mechanisms mentioned is the primary step of interface formation, whether it begins by the formation of a ternary GIC or by the electrochemical reduction of electrolyte on the surface. It is generally accepted that there is a

certain amount of solvent cointercalation during the formation of the SEI, however, further experimental studies are needed for confirmation.

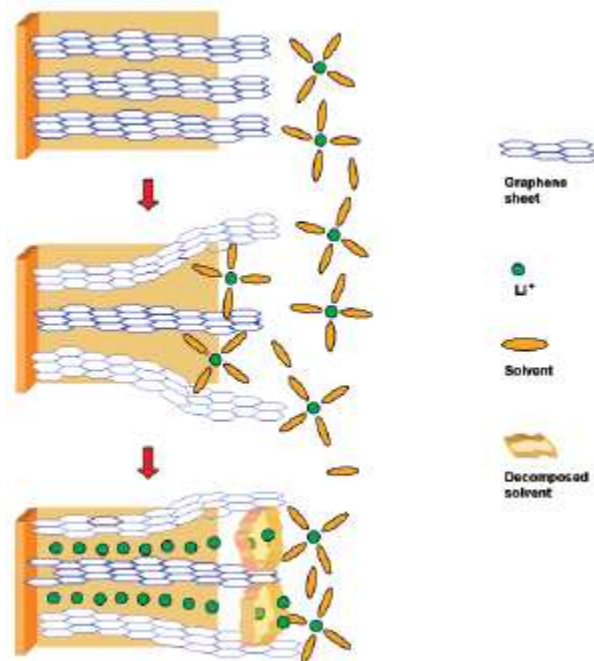


Figure 7. Schematic of SEI formation based on Besenhard's model [2]

1.6 THERMODYNAMICS OF ELECTROLYTES

In order to find the correct mixture between cosolvents, the temperature range of the electrolyte solutions also has to be kept in mind. This range would help serve as a basis for estimating operating limits that use the nonaqueous electrolyte system. As seen for the phase diagram in Figure 8, EC based electrolyte have varying temperature ranges based on their mole fraction with the co-solvent, which was performed by Ding, Xu, and Jow [29]. The liquidus line is characterized by the V-shape at which one of the components crystallizes in a binary system. Below the solidus line, characterized by the horizontal line, the whole system is in the solid phase. Between the solidus and liquidus line are regions at which both solid and liquid phases exist in the system. In order for the system to be in completely liquid phase, it must be above the

liquidus line. From the phase diagram, one of the more popular solvent combinations for lithium-ion, $\text{LiPF}_6/\text{EC}/\text{DMC}$, has a eutectic point at -7.6°C with molar fractions of 0.3 EC and 0.7 DMC. This is of concern for EC/DMC as the temperature limit is rather high when considering low temperature applications. Even the replacement of DMC with EMC, which has a lower melting point at -53°C , does not significantly improve the area of the liquid phase in a binary system. This shows that simply introducing a low melting point component does not result in extension of the liquid range. The low temperature application will remain a challenge as long as the high melting point of EC remains as a solvent component for lithium-ion electrolytes, due to its heavy influence on the liquid phase irrespective of which cosolvents are used.

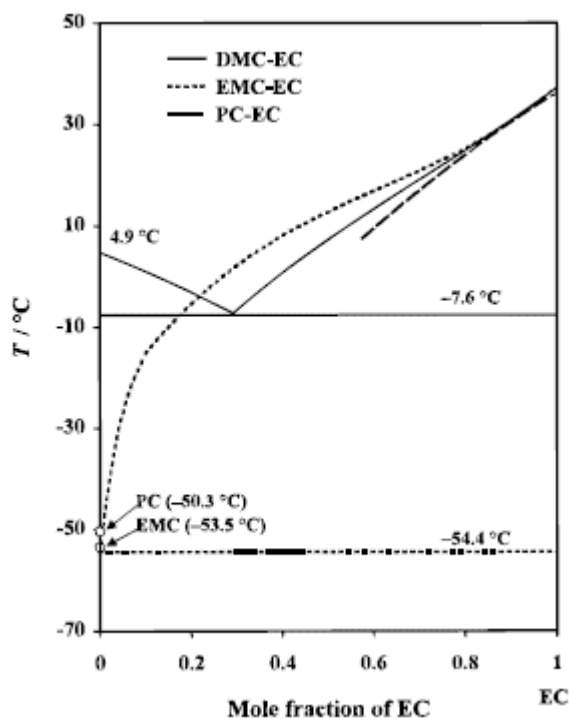


Figure 8. Phase Diagram of EC-based electrolyte [29]

Considering the phase diagram just mentioned, it only takes into account the thermal properties of solvents, while in application, the salt concentration also has an effect on the phase diagram

and is of importance. Ding, Xu, and Jow also studied the effects of salt on the liquidus and solidus line locations at various concentrations for LiPF_6 , as seen below in Figure 9 [29]. It was concluded that both lines were lowered with increasing salt concentrations. At the salt concentrations investigated, the general curve of the phase diagram remain unchanged.

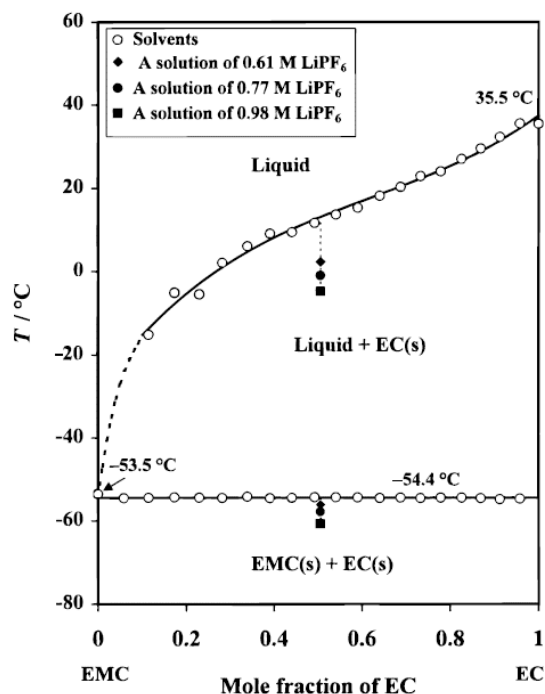


Figure 9. Phase diagram of EMC-EC with different LiPF_6 salt concentrations [29]

As research continues and lithium-ion batteries are commercialized for a wide range of applications, electrolyte composition will differ from one to another. However, the majority of these electrolyte are comprised of EC with one or more linear carbonates as the solvent and LiPF_6 as the solute. Certain battery performances are still problematic to this day even with the latest electrolyte combinations. This includes issues with low temperature performance due to EC's high melting point and liquidus temperature, as well as a high temperature performance impeded by LiPF_6 due to its reactivity with solvents.

1.7 ELECTROLYTE ADDITIVES

Due to the importance of the SEI formation on carbon based anodes and the abundance of research for different cosolvents have not shown much improvement, additives were also explored. Rather than replacing the main components of current electrolytes that could cause more problems, an alternative means is to modify certain functions by incorporating small concentrations of a new component, or additive, so that the potential impact on existing electrolyte is minimal. This would still have the benefits of the bulk properties of the main electrolyte components, but with the added effect of possibly changing unique properties. Additives have been used before in lithium batteries in an effort to subdue dendrite growth. Since the concept of the SEI, emphasis has been on the preferential decomposition of additives and the effect of the products on the SEI layer. Specific functions of additives for lithium-ion batteries include improving the ion conductivity properties in the bulk electrolyte, SEI layer modification, and prevention of overcharge on the battery.

One such additive that was used in this study is VC solvent, or vinylene carbonate. This solvent additive is the most used within the industry and was proposed initially by SAFT [25]. VC additive has been the subject of many studies recently. Although studies have shown the beneficial role of VC on the SEI layer, the exact mechanism of modification on the surface chemistry is still not clear. It is generally received that the reactivity of VC stems from its ability to polymerize from its vinyl functionality and the high strain from its structure. VC additive has been shown to effectively reduce the irreversible capacity associated with PC-based electrolyte, as well as not having any instability on charged surface of anode or cathode. It is suggested that VC addition to the electrolyte changes the SEI layer formed at the electrode/electrolyte interface upon decomposition and inhibits the parasitic reactions at the interface [24]. Aurbach et al.

investigated the effect of VC in ethylene carbonate based electrolyte on the negative electrode and reported that the additive increases cyclability, heat resistance, and decreases irreversible capacity [26]. They analyzed the surface chemistry of VC on graphite by the C1s and F1s spectra via XPS. As shown in Figure 10, the presence of VC reduced the content of LiF in the SEI, signified by the signal at 685 eV. The peak shown at 687 eV is mainly contributed to PVDF (polyvinylidene fluoride binder) with the LiF peak only showing as a small shoulder, whereas VC-free electrolyte shows LiF as the predominant species. In addition, there seems to be an increase of lithium alkyl carbonates (signal at 289 eV) with VC concentration.

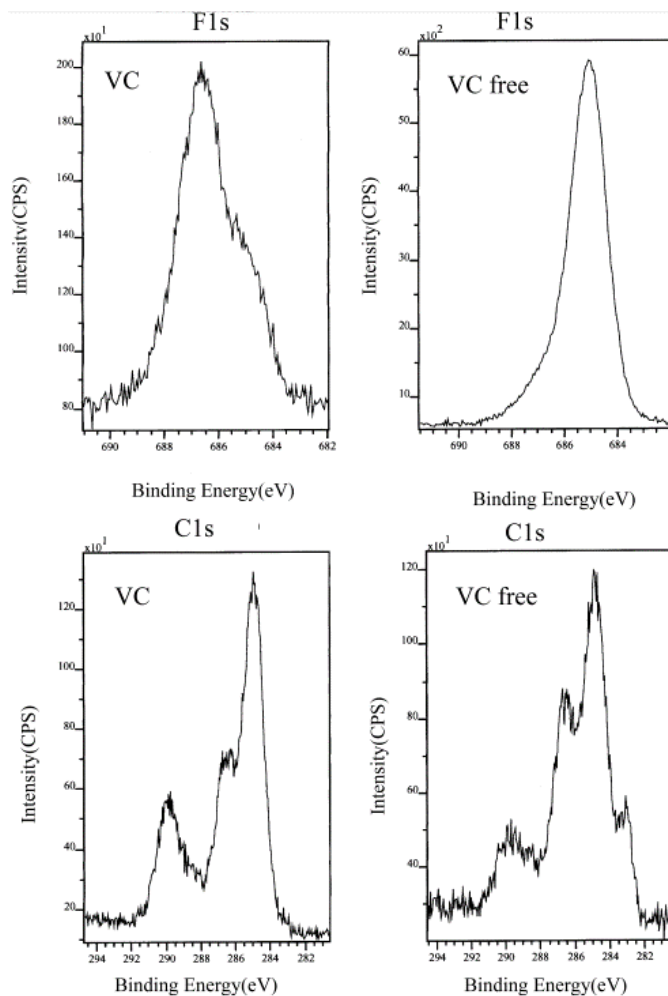
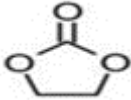
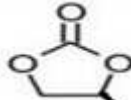
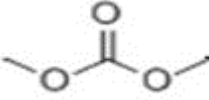
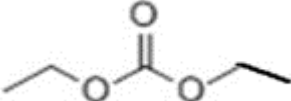
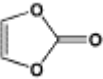


Figure 10. XPS spectra of VC and VC-free additive in EC-based electrolyte [26]

They proposed that VC additive polymerizes on the graphite surface, forming poly alkyl Li-carbonate species that suppresses solvent and salt anion reduction. Additionally, surface films containing polymers are expected to be more cohesive and flexible, which would provide better passivation as opposed to surface films containing Li salts. Even with different lithium-ion chemistries, VC has been shown to improve electrochemical behavior, cycling performance, and thermal stability. Furthermore, VC was seen to have added benefits at the cathode interface. In a study by Takamatsu et al., they found that adding VC to the electrolyte significantly improved the reversibility of the electronic structure at the cathode surface during subsequent charge/discharge cycles [27]. They attributed this to the formation of decomposed VC layer at the cathode/electrolyte interface, which helped in mitigating degradation of the capacity and the increase in resistance. The main advantage of VC additive is its preferential reduction, before the cointercalation of solvent, due to their higher reductive potential. The comparison between VC additive and other solvents can be seen below in Table 3. EC solvent has a reduction potential of 0.9 on glassy carbon (GC), PC at 1.0, DMC at 1.32, and DEC at 1.32. These solvents have a lower reduction potential than VC additive at 1.4, allowing VC to have preferential reduction and reduced on the anode surface before the bulk electrolyte components are involved. Collectively, many believe that VC was an effective additive for chemical modification of the anode SEI.

Table 3. Reduction Potentials of Solvents and Additives

| Solvent | Structure | Reduction Potential (vs. Li ⁺ /Li) |
|---------|--|---|
| EC |  | 0.9 |
| PC |  | 1.0 |
| DMC |  | 1.32 |
| DEC |  | 1.32 |
| VC |  | 1.4 |

There has also been research done in the pursuit of new lithium salts, due to the thermal instability of current electrolytes. Two major properties in seeking a potential salt is the thermal and chemical inertness for replacement, however, sometimes these improvements come at the consequence of other properties that are just as important for the operation of a lithium-ion battery. One such type of salt was lithium borates with nonaromatic ligands, which are synthesized by a series of borate anions chelated by various alkyl-based ligands. In comparison with aromatic ligands that has had extensive research, these salts had a much higher ion conductivity and anodic stability, while maintaining thermal stability. Among these new lithium borates, salts based on oxalato ligands were of particular interest. The salt, called lithium bis(oxalato)borate, or LiBOB for short, was invented by Lischka and other researchers [39]. Xu et al. found that LiBOB in mixed carbonate solvents was able to meet all the requirements for

electrolyte solute used for lithium-ion battery applications [40-41]. In their research, LiBOB showed comparable or better performances to LiBF_4 , LiClO_4 , and LiPF_6 . Lithium-ion cells containing this salt as electrolyte solute exhibited stable performance even at 60°C , something LiPF_6 is unable to achieve, which they concluded was due to the anion containing no labile fluorine. Additionally, Xu reported that LiBOB can effectively stabilize graphite anode materials from exfoliation in PC based electrolyte while supporting reversible lithium ion intercalation/deintercalation. For graphite anodes in PC-based electrolytes, exfoliation is characterized by a process occurring at 0.80V vs. Li. As seen below in Figure 11, while this exfoliation proceeds, the potential of the cell remains at a steady plateau and is never able to reach the lithium ion intercalation potential below 0.3V . This plateau is evident at $\sim 0.80\text{V}$ in all salt anion variations tested except for LiBOB, where it is the only salt that successfully forms a protective film on graphite during the first lithiation and prevents exfoliation in PC electrolyte.

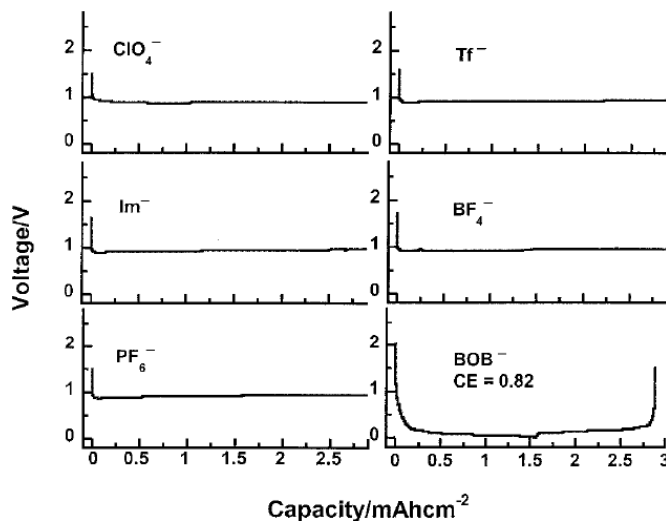


Figure 11. Profiles of Li/graphite half-cells containing various salts in PC-based electrolyte [41]

To understand how LiBOB electrolyte was able to stabilize graphitic anode and demonstrate thermal stability at high temperatures, Xu investigated the SEI layer formed on graphite via XPS

analysis [42]. In his findings, represented in Figure 12, they attributed the improvements to stem from the increase in compounds containing carbonyl moieties (semicarboxylate) due to decomposition of the BOB anion. This high abundance peak of semicarboxylate species has never been observed before for LiPF_6 based electrolytes.

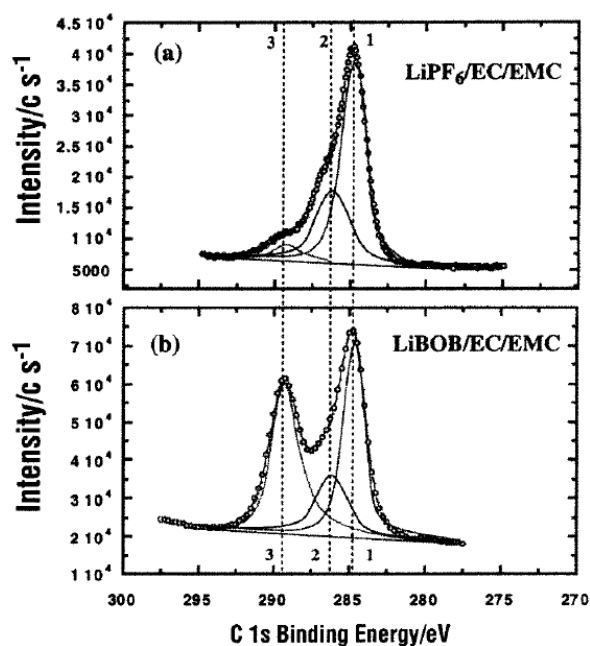


Figure 12. XPS C1s spectra for graphitic anode cycled in LiPF_6 and LiBOB based electrolytes [42]

Through much research, LiBOB has proven to be thermally stable, which is advantageous compared to the industry standard of LiPF_6 . Additionally, LiBOB has shown to be economical in terms of manufacturing cost and environmentally friendly by decomposing into less corrosive products. This novel salt has been proposed as a standalone electrolyte or in combination with other salts in order to operate at a much wider temperature range.

1.8 REMARKS ON CURRENT STATE OF LITHIUM-ION ELECTROLYTES

In summary, lithium-ion batteries are the latest state-of-the-art electrochemical energy storage devices used in consumer electronics, electric vehicles, and space exploration. Fast charging and discharging, long calendar life, long cycle life, and operation over a wide temperature range (-30°C to $+60^{\circ}\text{C}$) are some of the important properties desired for vehicle applications. A state-of-the-art LIB, even with its superior high energy density and rate capability in comparison to other battery chemistries, lacks the high power ability at low temperature. Recent understandings reveal the importance of investigating electrolyte formulations and chemical compositions as it directly affects cell performance in many aspects.

There are still issues in irreversible capacity, temperature limits, safety, and ion transportation when trying to find the perfect electrolyte system. Due to SEI formation, a certain amount of electrolyte is permanently consumed thereby having a loss of lithium ions, which are then immobilized in the form of insoluble salts. As most lithium-ion batteries are built as a cathode-limited design to avoid lithium metal deposition on carbon anode at the end of charging, the consumption of the lithium ions at the initial stages end in permanent capacity loss of the battery. The extent of the irreversible capacity depend on the anode material and the electrolyte composition. As previously discussed, PC is well-known to cause exfoliation of graphene on the anode which leads to irreversible capacities. In addition, changes in the electrolyte could help mitigate irreversible capacities, but consequently causing issues elsewhere. Another problem facing improvements in electrolytes is temperature limits. Two important components in present-day electrolytes are LiPF_6 and EC as salt and solvent, respectively. Although beneficial as evidenced previously, these two electrolyte components are sensitive to temperature extremes, therefore having these ingredients will impart temperature limits during the operation of lithium-

ion batteries. EC solvent is responsible for the lower temperature thresholds as it reduces the conductivity. LiPF_6 is responsible for the higher temperature extremes, typically above 60°C , which can limit the applications for certain industries. LiPF_6 is known to act as an initiator or catalyst for various decompositions involving the electrolyte, electrode, and SEI layer. Thirdly, safety is another potential issue facing today's lithium-ion electrolyte due to the use of certain solvents. Linear carbonate solvents are known to be highly flammable with low flash points, which can cause thermal runaway. Lastly, improvements in ion conductivity leaves much to be desired, as the conductivity is much lower compared with aqueous solutions. Enhancements in bulk ion conductivity could lead to a more conductive SEI layer.

In this study, 1.0 M LiPF_6 solution was used in various combinations of EC, PC, DMC, EMC, and DEC. The goal of this work was to optimize the cell performance for both low and high temperature using the conventional electrolyte system. Vinylene carbonate (VC) and lithium bis(oxalato)borate (LiBOB) were used as additives in 1 % and 0.5% weight ratio, respectively in all the electrolytes tested.

CHAPTER 2 – METHODOLOGY

2.1 SAMPLE PREPARATION

2.1.1 COIN CELL FABRICATION

Lithium hexafluorophosphate (LiPF_6 , 99.99%), battery grade lithium bis(oxalato)borate (LiBOB), and vinylene carbonate (VC , 99.5%, acid < 200 ppm, H_2O < 100 ppm) were purchased from Sigma Aldrich and used without further purification. EC, PC, DMC, EMC and DEC solvents were purchased from BASF Corporation and used without further treatments. In the NMC 111 cathode laminate, the loading of the active material was 6.80 mg/cm^2 (reversible capacity of 0.93 mA/cm^2). Graphite anode laminate was prepared with loading at 3.25 mg/cm^2 . Celgard 2325 polymer was also used as separator.

Using our knowledge of electrolyte properties, literature, and past experiments, we adopted a DOE (design of experiments) for use in electrolyte optimization. Design of experiments is a systematic technique that evaluates the relationship between the factor(s) affecting a process and the output of that process. In this case, the factors are the different electrolyte combinations which can change the components of the SEI layer, thus resulting in different discharge capacity performances. As seen below in Table 4, we had an upper and lower boundary limit for each solvent used in this study. EC was set between 20-30%, PC between 5-30%, EMC between 0-70%, DMC between 0-40%, and finally DEC between 0-40%.

Table 4. Electrolyte bounds used for DOE

| Electrolyte Bounds | | |
|--------------------|-------|-------|
| Component | Lower | Upper |
| EC | 20 | 30 |
| PC | 5 | 30 |
| EMC | 0 | 70 |
| DMC | 0 | 40 |
| DEC | 0 | 40 |

All the electrolyte preparation was done in an argon filled glovebox ($\text{H}_2\text{O} < 0.5$ ppm, $\text{O}_2 < 50$ ppm). A mixture of 10.0 grams of solvent combination (EC, PC, EMC, DMC, and DEC) at various ratios were prepared. A total of 43 combinations were investigated. Table 5 outlines the different electrolyte variations by weight percentage. The EC concentration was fixed between 20 to 30% by weight. PC was used between 5 to 30% by weight. The rest of the solvent mass was filled with linear carbonates (DMC, EMC, and DEC). LiPF_6 , (1.51 g) salt was added to each of the solvent composition to make 1.0 M solution. In each of the solutions, 0.11 gram of vinylene carbonate and 0.057 gram of LiBOB was also added to make 1% and 0.5% by weight of the electrolyte as additive, respectively. The electrolytes were left overnight to allow to dissolve completely.

Four replicates of coin cells were made using each electrolyte. Circular pieces of electrodes (cathode: 9/16 inch, anode: 5/8 inch in diameter) and 50 μL of electrolyte was used in each coin cells. The crimped coin cells were taken out from the glove box and stored at 25°C for 24 hours in a temperature controlled chamber.

A commercially available and widely used electrolyte (1.2 M LiPF₆ in 3/7 EC: EMC + 2 % VC) was also made for comparison purposes. Similarly, 1.0 M LiPF₆ solution in EC/PC/EMC (3:2:5) was made and CsPF₆ additive was added in it to make a 0.05 M concentration [49]. EC free electrolyte, 1.2 M LiPF₆ in EMC with 2% VC was also prepared. These electrolytes were studied in coin cells in addition to the 43 electrolyte combinations.

Table 5. 1.0M LiPF₆ Electrolytes with solvent variations and 1% VC/0.5% LiBOB as additive

| Electrolyte No. | EC | PC | EMC | DMC | DEC |
|------------------------|-----------|-----------|------------|------------|------------|
| 1 | 30.0 | 30.0 | 0.0 | 40.0 | 0.0 |
| 2 | 30.0 | 30.0 | 0.0 | 0.0 | 40.0 |
| 3 | 20.0 | 30.0 | 10.0 | 0.0 | 40.0 |
| 4 | 22.0 | 9.9 | 48.7 | 11.0 | 8.5 |
| 5 | 22.0 | 22.4 | 18.7 | 28.5 | 8.5 |
| 6 | 20.0 | 5.0 | 70.0 | 0.0 | 5.0 |
| 7 | 27.0 | 9.9 | 26.2 | 8.5 | 28.5 |
| 8 | 20.0 | 5.0 | 70.0 | 5.0 | 0.0 |
| 9 | 20.0 | 5.0 | 35.0 | 40.0 | 0.0 |
| 10 | 22.0 | 9.9 | 48.7 | 8.5 | 11.0 |
| 14 | 13.0 | 3.0 | 0.0 | 30.0 | 25.0 |
| 15 | 30.0 | 5.0 | 0.0 | 40.0 | 25.0 |
| 16 | 20.0 | 30.0 | 0.0 | 40.0 | 10.0 |
| 17 | 20.0 | 5.0 | 0.0 | 35.0 | 40.0 |
| 18 | 20.0 | 5.0 | 35.0 | 0.0 | 40.0 |
| 19 | 30.0 | 5.0 | 0.0 | 25.0 | 40.0 |
| 20 | 30.0 | 5.0 | 25.0 | 0.0 | 40.0 |
| 21 | 20.0 | 30.0 | 0.0 | 10.0 | 40.0 |
| 22 | 25.0 | 5.0 | 70.0 | 0.0 | 0.0 |
| 23 | 30.0 | 5.0 | 65.0 | 0.0 | 0.0 |
| 24 | 20.0 | 10.0 | 70.0 | 0.0 | 0.0 |
| 25 | 20.0 | 30.0 | 50.0 | 0.0 | 0.0 |
| 26 | 30.0 | 30.0 | 40.0 | 0.0 | 0.0 |
| 27 | 30.0 | 5.0 | 25.0 | 40.0 | 0.0 |
| 28 | 20.0 | 30.0 | 10.0 | 40.0 | 0.0 |

| | | | | | |
|-----------|------|------|------|------|------|
| 29 | 24.0 | 14.8 | 27.4 | 16.9 | 16.9 |
| 30 | 27.0 | 22.4 | 13.7 | 8.5 | 28.5 |
| 31 | 22.0 | 9.9 | 13.7 | 28.5 | 26.0 |
| 32 | 27.0 | 9.9 | 13.7 | 28.5 | 21.0 |
| 33 | 22.0 | 22.4 | 13.7 | 28.5 | 13.5 |
| 34 | 27.0 | 22.4 | 13.7 | 28.5 | 8.5 |
| 35 | 22.0 | 9.9 | 13.7 | 26.0 | 28.5 |
| 36 | 22.0 | 9.9 | 31.2 | 8.5 | 28.5 |
| 37 | 27.0 | 9.9 | 13.7 | 21.0 | 28.5 |
| 38 | 22.0 | 22.4 | 13.7 | 13.5 | 28.5 |
| 39 | 22.0 | 22.4 | 18.7 | 8.5 | 28.5 |
| 40 | 24.5 | 9.9 | 48.7 | 8.5 | 8.5 |
| 41 | 27.0 | 9.9 | 46.2 | 8.5 | 8.5 |
| 42 | 22.0 | 12.4 | 48.7 | 8.5 | 8.5 |
| 43 | 22.0 | 22.4 | 38.7 | 8.5 | 8.5 |
| 44 | 27.0 | 22.4 | 33.7 | 8.5 | 8.5 |
| 45 | 22.0 | 9.9 | 31.2 | 28.5 | 8.5 |
| 46 | 27.0 | 9.9 | 26.2 | 28.5 | 8.5 |

2.1.2 XPS SPECIMENS

The cycled cells were discharged and taken to the argon filled glove box ($\text{H}_2\text{O} < 1.0$ ppm). They were disassembled and the anode was cut into 4 pieces. The electrodes were then rinsed twice with small amounts of DMC. DMC is used to remove residual electrolytes and polymer-like interphasial species from electrodes [57]. The wash solvent (DMC) was removed from the electrode surface by evacuating them overnight. Samples were then mounted onto a flat cylindrical sample holder via double-sided carbon tape and allowed to vacuum overnight.

2.1.3 XRD SPECIMENS

Similarly with the XPS specimens, the XRD samples were taken from the cycled cells and prepped in an argon filled glove box ($\text{H}_2\text{O} < 1.0$ ppm). They were disassembled and the anode was cut into 4 pieces. The electrodes were then rinsed twice with small amounts of DMC.

The wash solvent (DMC) was removed from the electrode surface by evacuating them overnight. Samples were then mounted with double-sided tape in an airtight specimen holder ring. The holder ring was then sealed with a dome shaped x-ray transparent cap.

2.2 CHARACTERIZATION TECHNIQUES

Different characterization techniques were used in this study to examine the effect on electrolyte composition at different temperature ranges. This includes electrical performance testing, XPS, and XRD.

2.2.1 ELECTRICAL PERFORMANCE TESTING

In order to measure the effective capacity of each electrolyte at a certain temperature, electrical performance testing was done. The cycle performance of different electrolytes containing coin cells were measured using custom built Arbin Battery testing equipment. The procedures were designed to represent the battery duty cycles in a micro-hybrid vehicle. Each coin cell had the theoretical total capacity of 1.39 mAh. All charge/discharge experiments were done in constant current and constant voltage (CCCV) mode. First, the cells were charged by constant current until the voltage reaches to 4.1 V. Then, voltage was held constant at 4.1 V until the current value decayed to $C/20$. They were then discharged at a constant current of $C/5$ until the voltage reached 2.7 Volts. This cycle was completed 2 times. Then, a constant current, constant voltage charge/discharge cycle at a rate of 1C were applied between 2.0 V and 4.1 V for three cycles as part of the condition step. Between each charge and discharge cycle a one minute rest period was given. The entire formation and conditioning process was completed at 25°C. Afterwards, the cells were charged at 1C rate and discharged at 5C rate at room temperature. Following this, the cells were again charged with a 1C rate and then cooled at -20°C for 2 hours

and then discharged at a 5C rate. The cells were then warmed up to 25°C, kept at this temperature overnight and then charged at 1C. After the charge was completed, the cells were cooled to -30°C for 2 hours and discharged at a 5C rate. The cells were then warmed to 25°C and allowed to stay at this temperature overnight. These cells were then held at 60°C and cycled for 100 cycles at a 1C charge and 5C discharge rate. At the end of the 100 cycles, the -20°C and -30°C cycles were repeated. Then the above process of cycling (hot and cold) was repeated one more time. A total of 200 cycles at 60°C and 3 cycles at -20°C and 3 cycles at -30°C were performed.

Graphical representations can be seen below for formation, charge and discharge at room and low temperature (-20°C and -30°C), and 60°C cycling. As can be seen from Figure 13 below, formation involves 2 cycles of CCCV to 4.1V and discharge to 2.7V, followed by a conditioning step of 1C charge and discharge between 2.0V and 4.1V. Figures 14 and 15 shows a typical charge and discharge for room temperature and low temperature profiles. As stated earlier, the cell has a CCCV charge 1C rate until 4.1V, then held at 4.1V until current decays to C/20, followed by 2 hour rest at the temperature to be tested (1 minute for room temperature), then discharged at 5C rate until 2.0V. A closer look at Figure 16 shows how the discharge capacity is determined for this study, as they are measured at 2V after 5C discharge at their respective temperature. For 60°C cycling, only 7 cycles has been shown of the 200 cycles each electrolyte goes through in Figure 17. A tabulated version can also be seen in Appendix C outlining all cycling each cell goes through.

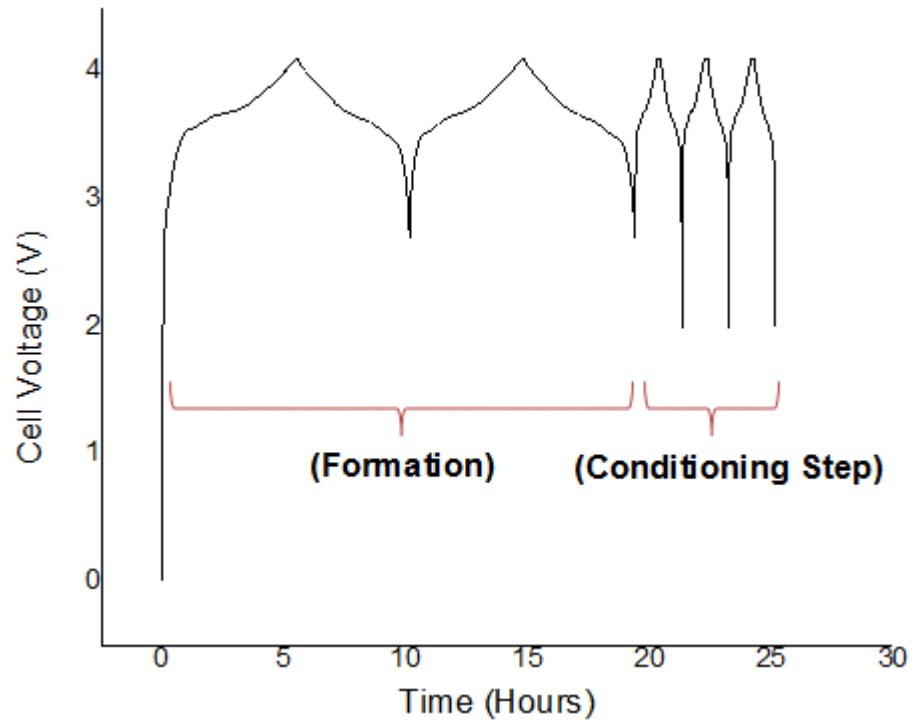


Figure 13. Formation cycles and condition step at room temperature. CCCV $C/5$ charge until 4.1V, held at 4.1V until $I=C/20$, then 1 minute rest, followed by $C/5$ discharge to 2.7V (2 cycles). Lastly, CCCV $1C$ charge until 4.1V, held at 4.1V until $I=C/20$, then 1 minute rest, followed by $1C$ discharge to 2.0V (3 cycles).

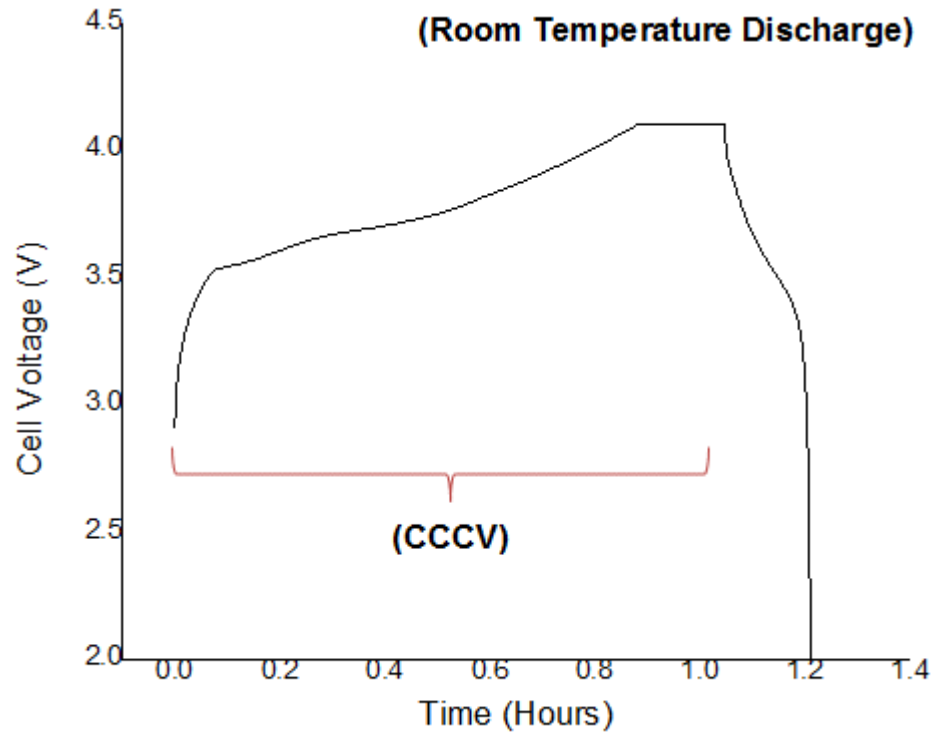


Figure 14. Representative room temperature cycling. CCCV 1C charge until 4.1V, held at 4.1V until $I=C/20$, then 1 minute rest, followed by 5C discharge to 2.0V.

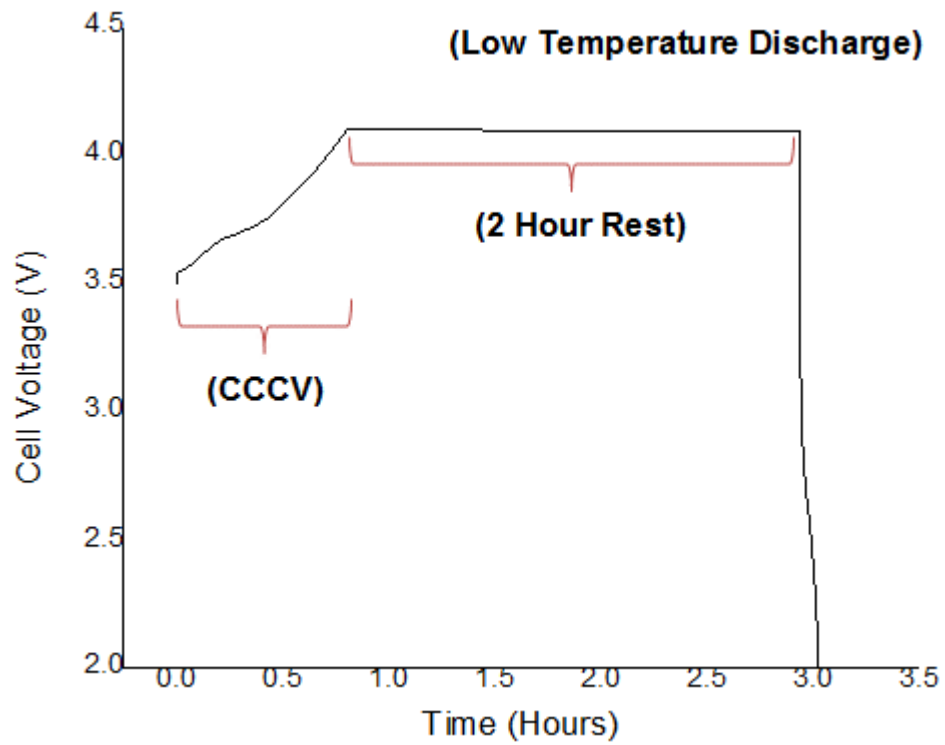


Figure 15. Representative -20°C and -30°C cycling. CCCV 1C charge until 4.1V, held at 4.1V until I=C/20, then 2 hour rest, followed by 5C discharge to 2.0V.

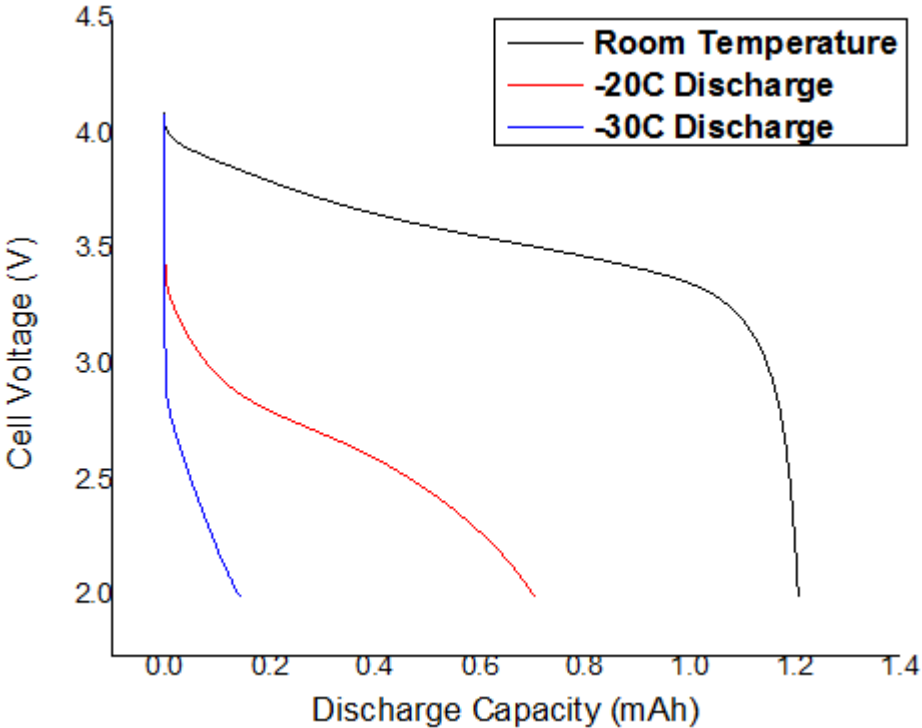


Figure 16. Representative room temperature, -20°C, and -30°C Discharge. Cells were discharged at 5C rate to 2.0V.

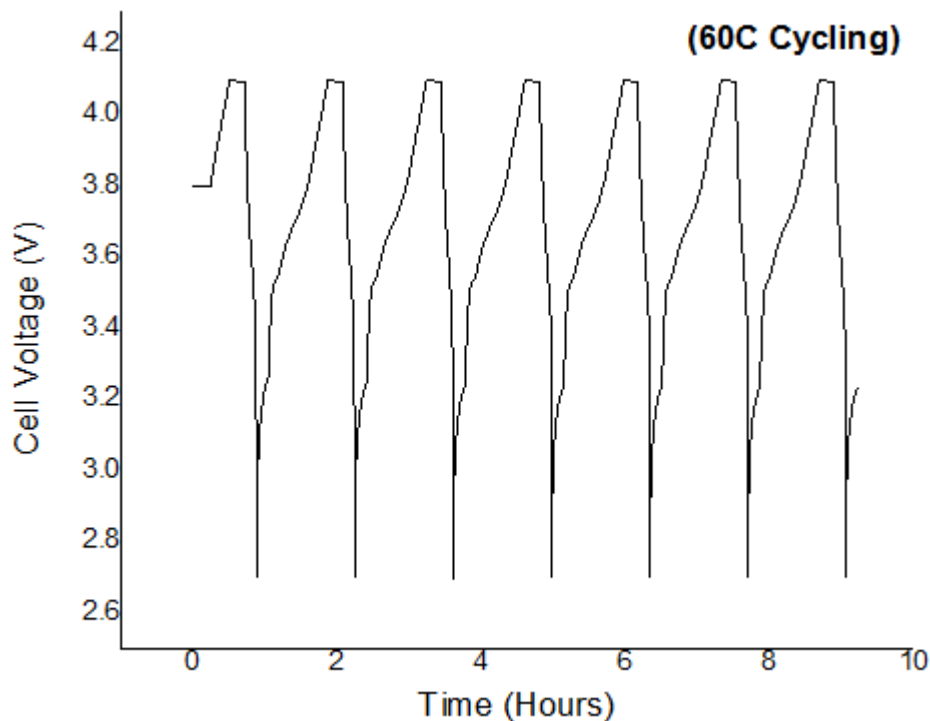


Figure 17. Representative 60°C cycling repeated for 100 cycles. CCCV 1C charge until 4.1V, held at 4.1V until $I=C/20$, then 10 minute rest, followed by 5C discharge to 2.7V.

AC-impedance tests were also performed on the cells in the charged state after the formation cycles, but before cycling. The impedance tests were conducted at 25°C and -20°C by Metrohm electrochemical workstation.

2.2.2 X-RAY PHOTOELECTRON SPECTROSCOPY (XPS)

XPS technique was used for this study to help identify the SEI components and is able to analyze the surface chemistry of a material. This technique can measure the elemental composition, empirical formula, chemical state, and electronic state of elements within a material. This technique works by having an X-ray beam excite the sample surface causing photoelectrons to be emitted. The resulting XPS spectra is obtained by measuring the kinetic energy and number of electrons that are emitted from the surface of the material. The kinetic

energy of the electron depends on the photon energy and the binding energy of the electron, or the energy required to remove the electron from the surface. The binding energy depends on a few factors, such as the element from which the electron is emitted, the orbital from which the electron is ejected, and the environment of the atom from which the electron is emitted. The energies and intensities of the peaks enable identification and quantification of the surface elements from the sample.

The number of detected electrons in each peak is directly related to the amount of elements in the sample. In order to generate atomic percentage, each XPS signal should be normalized by dividing its signal intensity by a relative sensitivity factor.

XPS spectra of the anode surface were collected using Perkin-Elmer PHI 5400 system using Mg radiation. For X-ray source setup, the pressure in the analysis chamber was $<5 \times 10^{-9}$ Torr based on the digital gauge control readout. In order to count the number of electrons with minimal error, the XPS detector must be operated under vacuum conditions as there is a long path length for detection of the irradiated material which requires low pressures. The X-ray source was used at 14.5 kV. C1s, F1s, O1s, and P2p spectra were calibrated using C-C peak at 284.3 eV as a reference. The elemental concentrations were calculated by dividing the ratio of peak area to sensitivity factor (A/s) of each element by sum of the same ratios of all the elements ($\sum A/s$). Here, A is the XPS peak area of each element obtained from multiple scans and s is the sensitivity factor of the same element.

Table 6 shows the XPS settings that were used for the anode analysis. For the survey analysis, the upper limit for binding energy was set at 1000 and the lower limit set at 0. eV/step was ran at 1, pass energy at 89.45, time/step at 100, and a total of 5 sweeps using an aperture size of 4. Survey time took a total of 8.3 minutes. In the multiplex analysis, 4 different elements

were quantified, C1s, F1s, O1s, and P2p. All eV/steps, sweeps, time/step, pass energy and cycles were remained consistent throughout all electrolytes sampled. Survey scans are used to obtain qualitative elemental composition information of the sample which can be used to define narrower range multiplex scans, and in turn can then be used for composition and chemical state analysis.

Table 6. XPS settings for anode analysis

| Survey | | | | | | | | |
|--------|-------------|-------------|---------|-------------|-----------|--------|------|---------------|
| | Upper Limit | Lower Limit | eV/step | Pass Energy | Time/Step | Sweeps | Time | Aperture Size |
| Anode | 1000 | 0 | 1 | 89.45 | 100 | 5 | 8.3 | 4 |

| Multiplex - Anode | | | | | | | | |
|-------------------|----------------|-------------|---------|------------------|-------------|----------------|------------------------|------|
| Anode Element | Binding Energy | | eV/step | Acquisition Time | | Pass Energy | Total Acquisition Time | |
| | Upper Limit | Lower Limit | | Sweeps | Time / Step | | Cycles | Time |
| C 1s | 296 | 276 | 0.125 | 10 | 50 | 44.75 | 1 | 8.1 |
| F 1s | 695 | 675 | 0.125 | 20 | 50 | 44.75 | 1 | 8.1 |
| O 1s | 542 | 522 | 0.125 | 10 | 50 | 44.75 | 1 | 8.1 |
| P 2p | 140 | 120 | 0.125 | 20 | 50 | 44.75 | 1 | 8.1 |

2.2.3 X-RAY DIFFRACTION (XRD)

In this study, the crystallographic orientation of samples can be determined by using the XRD. X-ray powder diffraction technique identifies phases of a crystalline material and provides information on unit cell dimensions.

X-rays are generated by a cathode ray tube and directed toward the sample. Interaction of incident rays with the sample produces constructive interference at specific angles. In order for this to occur, Bragg's law must be satisfied, as seen in the equation below, where the plane normal must be parallel to the diffraction vector.

$$\lambda = 2d_{hkl}\sin\theta$$

Peak positions are then plotted which signify the space (d_{hkl}) between diffracting planes of atoms. The peak intensity is determined by what atoms are in the diffracting planes. Typically, XRD spectra is plotted out in 2θ , conversion to d_{hkl} allows for identification of the sample.

The cycled coin cell samples were tested on a Bruker D8 Discover model XRD (AXS GmbH 2000). XRD Commander software was used to scan the samples and measurement data acquisition. In addition, Diffrac.eva software was used for quantitative analysis and phase identification. The X-ray source used was a Cu tube with 1.54060 Å wavelength.

Samples analyzed had a detector slit opening of 0.1 mm. The X-ray generator was at 40 kV and 40 mA as standard power. Samples were scanned at 2θ values from 20° to 90° . Scan step size settings were at 0.020° and 5 seconds per step.

CHAPTER 3 – RESULTS AND DISCUSSION

3.1 ELECTRICAL PERFORMANCE TESTS

In order to find an electrolyte best suited for low temperature application, we've tested various combinations per the DOE at both -20°C and -30°C down to 2V. Table 7 shows a few representative electrolyte combinations out of all the electrolytes that were created and their low temperature performance after formation was complete. Additionally, Table 8 shows low temperature performance for electrolytes that were investigated apart from the DOE. The discharge rates for both -20°C and -30°C are reported at 5C.

Table 7. Representative low temperature performance for various electrolytes from DOE

| Electrolyte names | Solvent ratios | LiPF ₆ | Additives (1 % and 0.5%) | -20 °C (mAh) | -30 °C (mAh) |
|-------------------|--|-------------------|-----------------------------|-----------------|-----------------|
| 1 | EC/PC/EMC/DMC/DEC 30: 30: 0: 40: 0 | 1.0 M | VC+LiBOB | 0.0 | 0.0 |
| 2 | EC/PC/EMC/DMC/DEC 30: 30: 0: 0: 40 | 1.0 M | VC+LiBOB | 0.12 | 0.03 |
| 3 | EC/PC/EMC/DMC/DEC 20: 30: 10: 0: 40 | 1.0 M | VC+LiBOB | 0.27 | 0.04 |
| 4 | EC/PC/EMC/DMC/DEC 22: 9.9: 48.7: 11: 8.5 | 1.0 M | VC+LiBOB | 0.68 | 0.18 |
| 5 | EC/PC/EMC/DMC/DEC 22: 22.4: 18.7: 28.5: 8.5 | 1.0 M | VC+LiBOB | 0.12 | 0.03 |
| 6 | EC/PC/EMC/DMC/DEC 20: 5: 70: 0: 5 | 1.0 M | VC+LiBOB | 0.59 | 0.07 |
| 7 | EC/PC/EMC/DMC/DEC 27: 9.9: 26.2: 8.5: 28.5 | 1.0 M | VC+LiBOB | 0.37 | 0.05 |
| 8 | EC/PC/EMC/DMC/DEC 20: 5: 70: 5: 0 | 1.0 M | VC+LiBOB | 0.64 | 0.14 |
| 9 | EC/PC/EMC/DMC/DEC 20: 5: 35: 40: 0 | 1.0 M | VC+LiBOB | 0.74 | 0.35 |
| 10 | EC/PC/EMC/DMC/DEC 22: 9.9: 48.7: 8.5: 11 | 1.0 M | VC+LiBOB | 0.53 | 0.07 |

Table 8. Additional low temperature performance for various electrolytes

| Electrolyte names | Solvent ratios | LiPF ₆ | Additives | -20 °C (mAh) | -30 °C (mAh) |
|-------------------|-----------------------|-------------------|-------------------|--------------|--------------|
| Cs | EC/PC/EMC, 3:2:5 [49] | 1.0 M | CsPF ₆ | 0.41 | 0.11 |
| 11 | EC/EMC, 3:7 | 1.2 M | No additive | 0.50 | 0.15 |
| 12 | EC/EMC, 3:7 | 1.2 M | VC | 0.63 | 0.11 |
| 13 | EC/EMC, 0:1 [48] | 1.2 M | VC | 0.74 | 0.39 |

It can be clearly seen from the Table 7 and 8 that the low temperature discharge capacity was strongly dependent upon the solvent composition. When the sum of cyclic carbonates was more than 40% in the total mixture, the low temperature discharge capacity was adversely affected. Electrolyte 1, almost 60% of which had cyclic carbonates, did not deliver any discharge capacity. Similarly, electrolytes 5 and 2 had high percentage of cyclic carbonates and delivered very small discharge capacities at low temperatures. Electrolyte 3, composed of 40% DEC and 50% cyclic carbonates, demonstrated slightly improved low temperature discharge capacity (compared to electrolytes 5 and 2). However, when the percentage of EC, PC, and DEC decreased, the low temperature discharge capacity significantly increased (electrolytes 4, 6, 8, 9). Another distinct behavior can be noticed in Tables 7 and 8 was that most of the electrolytes that performed well at -20°C, failed to perform at -30°C. However, electrolytes 9 and 13 showed an exception, they demonstrated high capacity at -20°C (0.74 mAh) and -30°C (0.35 mAh or more). In electrolyte 9, there was small amount of PC/EC balanced with high amount of DMC/EMC. Interestingly, electrolyte 13 had no EC, PC, DMC, or DEC. It had only EMC as the solvent and still performed well in both instances. Electrolyte 12 showed better performance than electrolyte 11, with both having the same compositions (EC/EMC, 3/7), except electrolyte 11 has no VC additive whereas

electrolyte 12 has 2% VC. The presence of the additive had a significant positive effect on the low temperature performance. CsPF₆ additive (0.05 M) [49] had been reported to enhance the low temperature performance of lithium-ion battery electrolytes. The discharge capacities of the cell with CsPF₆ additive (labeled as Cs) at -20°C and -30°C were relatively moderate (0.41 mAh and 0.11 mAh respectively) in comparison with other electrolytes such as 12, 13, 9, 4, 8, etc.

Table 9 shows the remainder of the electrolytes that were investigated along with their -20°C and -30°C capacity performance. There are certainly differences in low temperature performance among the many electrolyte combinations which can be better depicted in figures below. Performances for second round of -20°C and -30°C has also been tabulated in appendix A.

Table 9. Remaining low temperature performance for various electrolytes from DOE

| Electrolyte names | Solvent ratios | LiPF ₆ | Additives (1 % and 0.5%) | -20 °C (mAh) | -30 °C (mAh) |
|-------------------|--|-------------------|-----------------------------|-----------------|-----------------|
| 14 | EC/PC/EMC/DMC/DEC 13: 3: 0: 30: 25 | 1.0 M | VC+LiBOB | 0.56 | 0.08 |
| 15 | EC/PC/EMC/DMC/DEC 30: 5: 0: 40: 25 | 1.0 M | VC+LiBOB | 0.43 | 0.06 |
| 16 | EC/PC/EMC/DMC/DEC 20: 30: 0: 40: 10 | 1.0 M | VC+LiBOB | 0.08 | 0.02 |
| 17 | EC/PC/EMC/DMC/DEC 20: 5: 0: 35: 40 | 1.0 M | VC+LiBOB | 0.27 | 0.04 |
| 18 | EC/PC/EMC/DMC/DEC 20: 5: 35: 0: 40 | 1.0 M | VC+LiBOB | 0.58 | 0.12 |
| 19 | EC/PC/EMC/DMC/DEC 30: 5: 0: 25: 40 | 1.0 M | VC+LiBOB | 0.53 | 0.08 |
| 20 | EC/PC/EMC/DMC/DEC 30: 5: 25: 0: 40 | 1.0 M | VC+LiBOB | 0.47 | 0.09 |
| 21 | EC/PC/EMC/DMC/DEC 20: 30: 0: 10: 40 | 1.0 M | VC+LiBOB | 0.22 | 0.05 |
| 22 | EC/PC/EMC/DMC/DEC 25: 5: 70: 0: 0 | 1.0 M | VC+LiBOB | 0.65 | 0.14 |
| 23 | EC/PC/EMC/DMC/DEC 30: 5: 65: 0: 0 | 1.0 M | VC+LiBOB | 0.63 | 0.11 |
| 24 | EC/PC/EMC/DMC/DEC 20: 10: 70: 0: 0 | 1.0 M | VC+LiBOB | 0.43 | 0.06 |

| | | | | | |
|----|---|-------|----------|------|------|
| 25 | EC/PC/EMC/DMC/DEC 20: 30: 50: 0: 0 | 1.0 M | VC+LiBOB | 0.43 | 0.08 |
| 26 | EC/PC/EMC/DMC/DEC 30: 30: 40: 0: 0 | 1.0 M | VC+LiBOB | 0.07 | 0.02 |
| 27 | EC/PC/EMC/DMC/DEC 30: 5: 25: 40: 0 | 1.0 M | VC+LiBOB | 0.45 | 0.08 |
| 28 | EC/PC/EMC/DMC/DEC 20: 30: 10: 40: 0 | 1.0 M | VC+LiBOB | 0.46 | 0.07 |
| 29 | EC/PC/EMC/DMC/DEC 24: 14.8: 27.4: 16.9: 16.9 | 1.0 M | VC+LiBOB | 0.41 | 0.06 |
| 30 | EC/PC/EMC/DMC/DEC 27: 22.4: 13.7: 8.5: 28.5 | 1.0 M | VC+LiBOB | 0.35 | 0.06 |
| 31 | EC/PC/EMC/DMC/DEC 22: 9.9: 13.7: 28.5: 26 | 1.0 M | VC+LiBOB | 0.52 | 0.04 |
| 32 | EC/PC/EMC/DMC/DEC 27: 9.9: 13.7: 28.5: 21 | 1.0 M | VC+LiBOB | 0.45 | 0.07 |
| 33 | EC/PC/EMC/DMC/DEC 22: 22.4: 13.7: 28.5: 13.5 | 1.0 M | VC+LiBOB | 0.46 | 0.05 |
| 34 | EC/PC/EMC/DMC/DEC 27: 22.4: 13.7: 28.5: 8.5 | 1.0 M | VC+LiBOB | 0.08 | 0.02 |
| 35 | EC/PC/EMC/DMC/DEC 22: 9.9: 13.7: 26: 28.5 | 1.0 M | VC+LiBOB | 0.64 | 0.13 |
| 36 | EC/PC/EMC/DMC/DEC 22: 9.9: 31.2: 8.5: 28.5 | 1.0 M | VC+LiBOB | 0.60 | 0.12 |
| 37 | EC/PC/EMC/DMC/DEC 27: 9.9: 13.7: 21: 28.5 | 1.0 M | VC+LiBOB | 0.14 | 0.03 |
| 38 | EC/PC/EMC/DMC/DEC 22: 22.4: 13.7: 13.5: 28.5 | 1.0 M | VC+LiBOB | 0.51 | 0.09 |
| 39 | EC/PC/EMC/DMC/DEC 22: 22.4: 18.7: 8.5: 28.5 | 1.0 M | VC+LiBOB | 0.17 | 0.03 |
| 40 | EC/PC/EMC/DMC/DEC 24.5: 9.9: 48.7: 8.5: 8.5 | 1.0 M | VC+LiBOB | 0.45 | 0.06 |
| 41 | EC/PC/EMC/DMC/DEC 27: 9.9: 46.2: 8.5: 8.5 | 1.0 M | VC+LiBOB | 0.55 | 0.09 |
| 42 | EC/PC/EMC/DMC/DEC 22: 12.4: 48.7: 8.5: 8.5 | 1.0 M | VC+LiBOB | 0.62 | 0.09 |
| 43 | EC/PC/EMC/DMC/DEC 22: 22.4: 38.7: 8.5: 8.5 | 1.0 M | VC+LiBOB | 0.09 | 0.02 |
| 44 | EC/PC/EMC/DMC/DEC 27: 22.4: 33.7: 8.5: 8.5 | 1.0 M | VC+LiBOB | 0.26 | 0.04 |
| 45 | EC/PC/EMC/DMC/DEC 22: 9.9: 31.2: 28.5: 8.5 | 1.0 M | VC+LiBOB | 0.59 | 0.10 |
| 46 | EC/PC/EMC/DMC/DEC 27: 9.9: 26.2: 28.5: 8.5 | 1.0 M | VC+LiBOB | 0.59 | 0.09 |

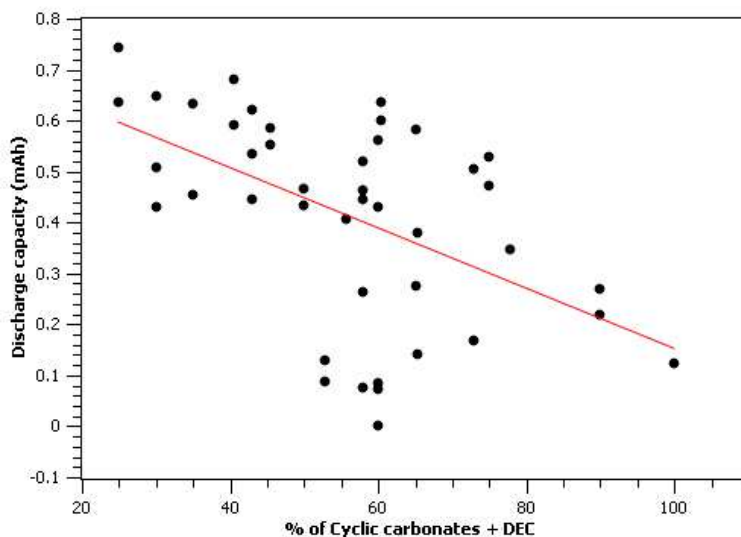


Figure 18. Discharge capacity of different electrolytes containing various amount of cyclic carbonates including DEC at -20°C. The rate of discharge is 5C.

Figure 18 shows the discharge capacity of various electrolytes at -20°C containing different amounts of cyclic carbonates. The trend clearly shows that as the content of cyclic carbonates increases, the low temperature discharge capacity decreases. In this experiment, the EC content was only varied from 20 to 30 percent, which makes it difficult to isolate the effect of varying only EC on the cold discharge capacity. Therefore, we can only show the effect of varying EC, PC, and DEC in combination together.

Figure 19 shows the impact of the concentration of short chain linear carbonates (and EC because of the reasons stated earlier) on the discharge capacity at low temperature. Apparently, as the amount of linear carbonates increased so did the low temperature performance. This was an unexpected result as we initially hypothesized that a higher percentage of these solvents wouldn't give better low temperature performance due to the freezing points of DMC and EC being high (3°C and 35°C, respectively). This leads us to believe that the electrolyte viscosity and conductivity plays a small role in cold temperature performance.

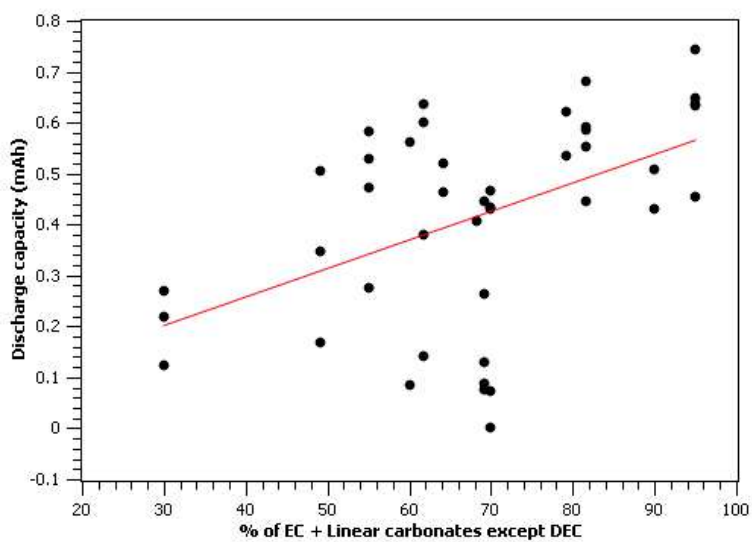


Figure 19. Discharge capacity of different electrolytes containing various amounts of short chain linear carbonates and EC at -20°C. The rate of discharge is 5C.

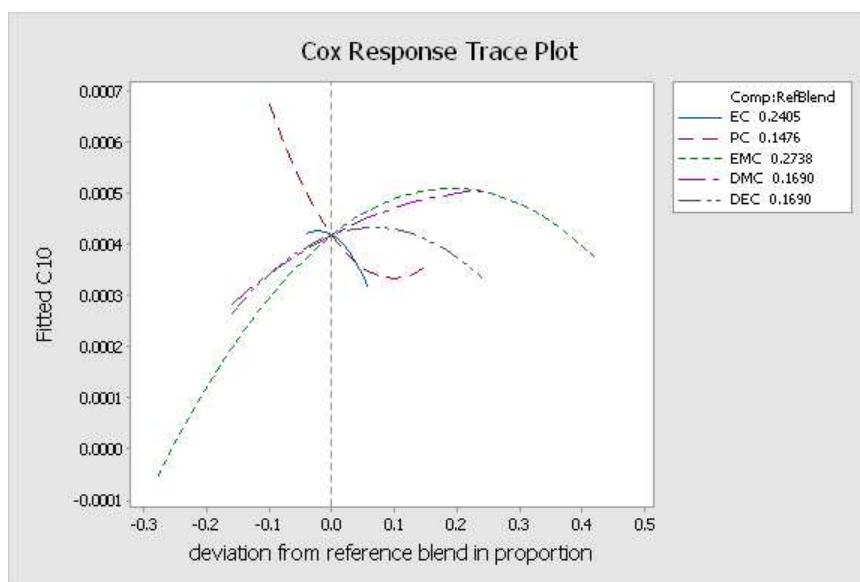


Figure 20. Cox response plot of discharge capacity for different electrolytes at -20°C. The rate of discharge is 5C.

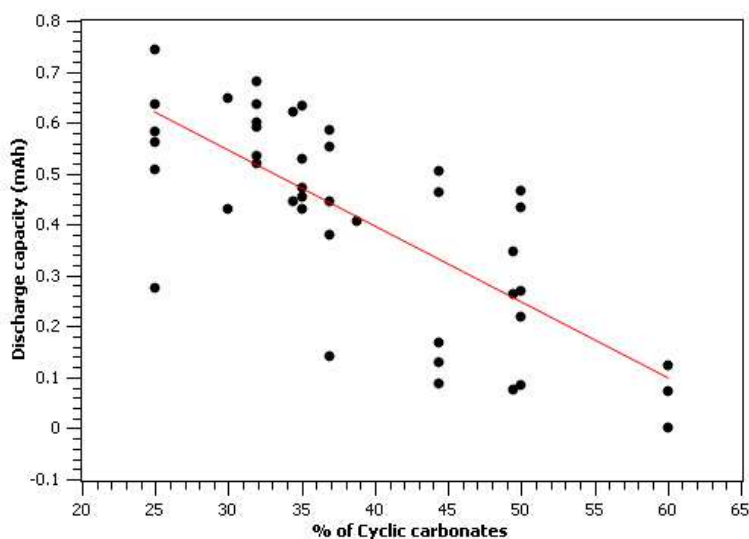


Figure 21. Discharge capacity of different electrolytes containing various amounts of cyclic carbonates at -20°C. The rate of discharge is 5C.

As mentioned earlier for the representative electrolytes, there is a strong correlation between lower amounts of cyclic carbonates leading to a better low temperature performance for the remaining electrolytes. This is evidenced by the Cox plot displayed in Figure 20 showing that performance will decrease when increasing in either EC (blue line) or PC (dashed red line) from the reference blend at ~24% and ~15%, respectively. In the same plot, an increase in the linear carbonates show better performance, however only up to a certain point, especially for EMC and DEC. Additionally, Figure 21 above shows discharge capacity versus the percent of cyclic carbonates only. Possibly the biggest hindrance for lower temperature performance is due to EC solvent, as it has a high melting point and its liquid range too restricted.

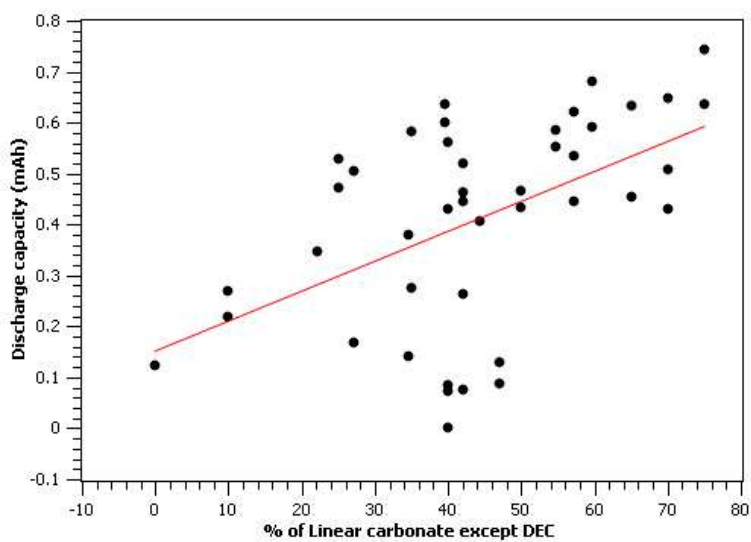


Figure 22. Discharge capacity of different electrolytes containing various amounts of linear carbonates except DEC at -20°C. The rate of discharge is 5C.

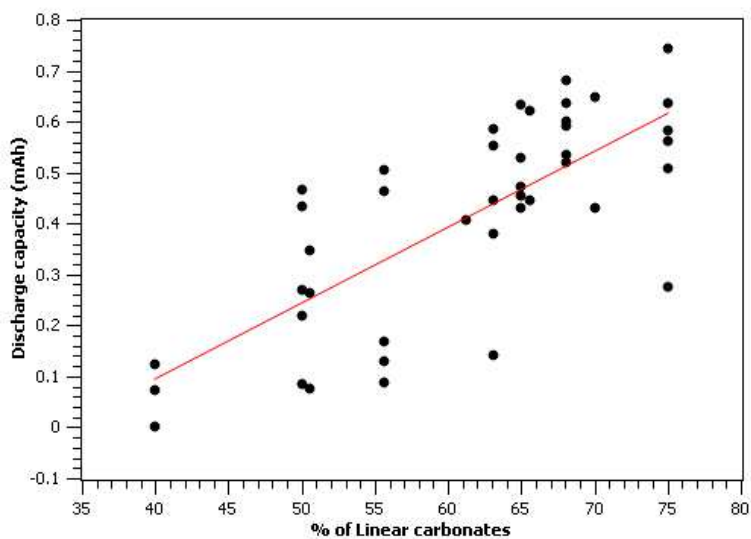


Figure 23. Discharge capacity of different electrolytes containing various amounts of linear carbonates at -20°C. The rate of discharge is 5C.

Figures 22 and 23 above also show the percentage of short linear carbonates only and all of linear carbonates used, respectively. There seems to be a correlation between percentages of carbonate to low temperature performance, as more linear carbonates contribute to a better performance. The same effect seems to happen with the addition of DEC solvent. However, when adding DEC solvent to other linear carbonates, there is only a slight change in slope as opposed to only having short linear carbonates. The addition of DEC suggests to have less of an impact for low temperature performance, as it may hinder the greater contribution coming from either EMC or DMC, or both.

To better understand how the discharge capacity is changed with differences in testing temperature and after 60°C cycling, we looked at the discharge curves for better interpretation. Figure 24A shows the discharge curves for the electrolyte 9 at 25°C, -20°C, and -30°C after their formation cycles. The electrolyte contains 40% of DMC along with EC (20%), PC (5%) and EMC (35%). The 5C rate discharge capacity at room temperature is about 1.26 mAh. However, the discharge capacity at -20°C and -30°C with 5C rate is 0.74 mAh and 0.35 mAh, respectively. A total of 59 % and 28% of the room temperature discharge capacity was retained at -20°C and -30°C, respectively. The IR drop at room temperature was 7.5 Ohms. The IR drop at -20°C and -30°C were 61.0 Ohms and 101.0 Ohms representing 8 times and 13 times increase, respectively. As can be seen, the large IR drop is mainly due to the lowering of the temperature, which then results in a lower overall discharge capacity. The shape of the discharge curve between room temperature and -20°C look very similar, however, once going down to -30°C, the shape of the discharge curve drastically changes.

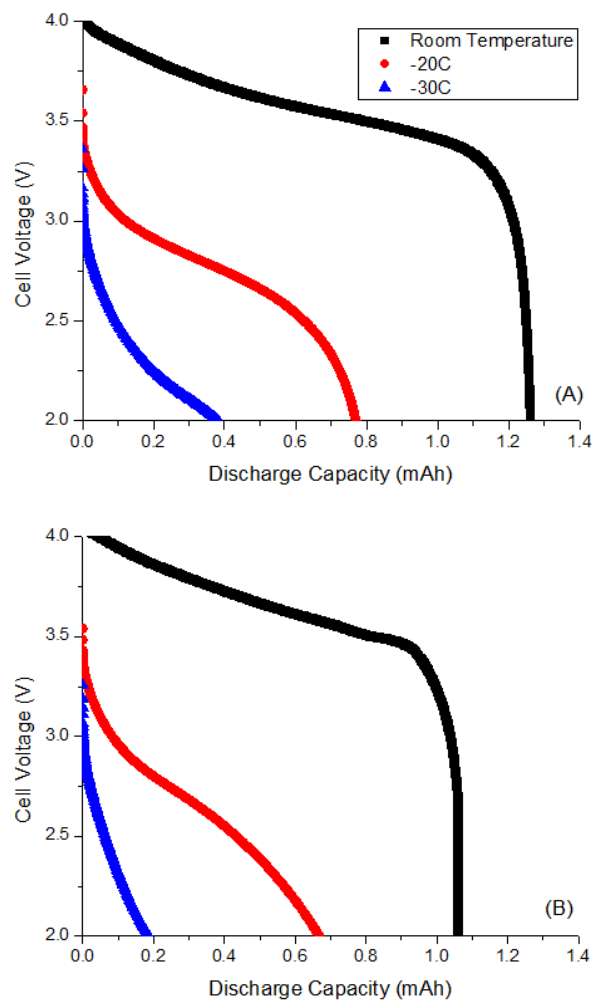


Figure 24. A) Discharge curves of the electrolyte 9 at 5C rate at room temperature, -20°C and -30°C after the formation is complete. The cells were cooled for 2 hours before being discharged; B) Discharge curves of the electrolyte 9 at 5C rate at -20°C and -30°C after 100 cycles at 60°C. The cells were cooled for 2 hours before being discharged. The capacity loss at -20°C and -30°C is about 9% and 50% respectively compared with the fresh cells.

The cells were then cycled at 60°C after completing the cold temperature discharge, as to mimic accelerated aging. The cell capacity decreased from 1.26 mAh to 1.05 mAh after 100 cycles at 60°C. The capacity loss was 15 to 20% of the initial capacity.

Figure 24B compares the discharge curves of the same cells at -20°C and -30°C (a second time) after they completed 100 cycles at 60°C. The 5C rate discharge capacities at -20°C and -30°C are 0.67 mAh and 0.18 mAh respectively. Comparing the fresh cells to those after 100 cycles

at 60°C, it was seen that the -20°C discharge capacity decreased just by 9%. However, the -30°C capacity decreased by roughly 50%. After one more thermo-cycle (100 cycles at 60°C), the cell delivered 0.51 mAh and 0.09 mAh capacity (69% and 26% of the initial low temperature capacity) at -20°C and -30°C, respectively. Evidently, electrolyte 9 retained its capacity well after 200 thermo-cycles (60/ -20 /-30°C).

Comparing the discharge values of electrolytes 11 and 12 in Table 8, electrolyte 12 had an increase in -20°C capacity by 26%, going from 0.50 mAh to 0.63 mAh. The difference between the two electrolytes was that electrolyte 12 had 2 % VC. It is worth to mentioning that the presence of 2 % VC in electrolyte did not change the conductivity of electrolyte. Furthermore, the majority of VC would be reduced during the formation process, thus having it act as a sort of sacrificial additive. Therefore, it can be assumed that the better low temperature performance may be more dependent on the quality of SEI than conductivity of the electrolyte.

Another interesting electrolyte was the EC free electrolyte, electrolyte 13 in Table 8 [48]. This electrolyte performed well in its initial low temperature discharge; 0.74 mAh at -20°C and 0.39 mAh at -30°C. However, after 100 cycles at 60°C, only half of the low temperature capacity was retained. It seems that EC is necessary for the stability of the SEI layer, especially at elevated temperatures.

The electrolyte with CsPF₆ additive was reported as a potentially good electrolyte for low temperature applications [49]. However, the electrolyte did not stand out among the electrolytes in our experiment protocol. The discharge capacity for fresh cells was only 0.41 mAh and 0.11 mAh at -20°C and -30°C, respectively.

3.2 X-RAY PHOTOELECTRON SPECTROSCOPY (XPS)

XPS technique was used for this study to analyze the surface chemistry of the anode in order to identify the SEI components. Figure 25 shows the comparison of the XPS spectra of two representative electrolytes (9 and 10) and a fresh un-cycled anode spectra (on the top). Electrolyte 9 showed very good low temperature results at -20°C and -30°C , at 0.74 and 0.35 mAh, respectively. Electrolyte 10 also showed good high temperature performance at 60°C during thermo-cycling showing 1.06 mAh discharge capacity, however did not perform as well as electrolyte 9 at low temperature with performance at 0.53 mAh and 0.07 mAh at -20°C and -30°C , respectively.

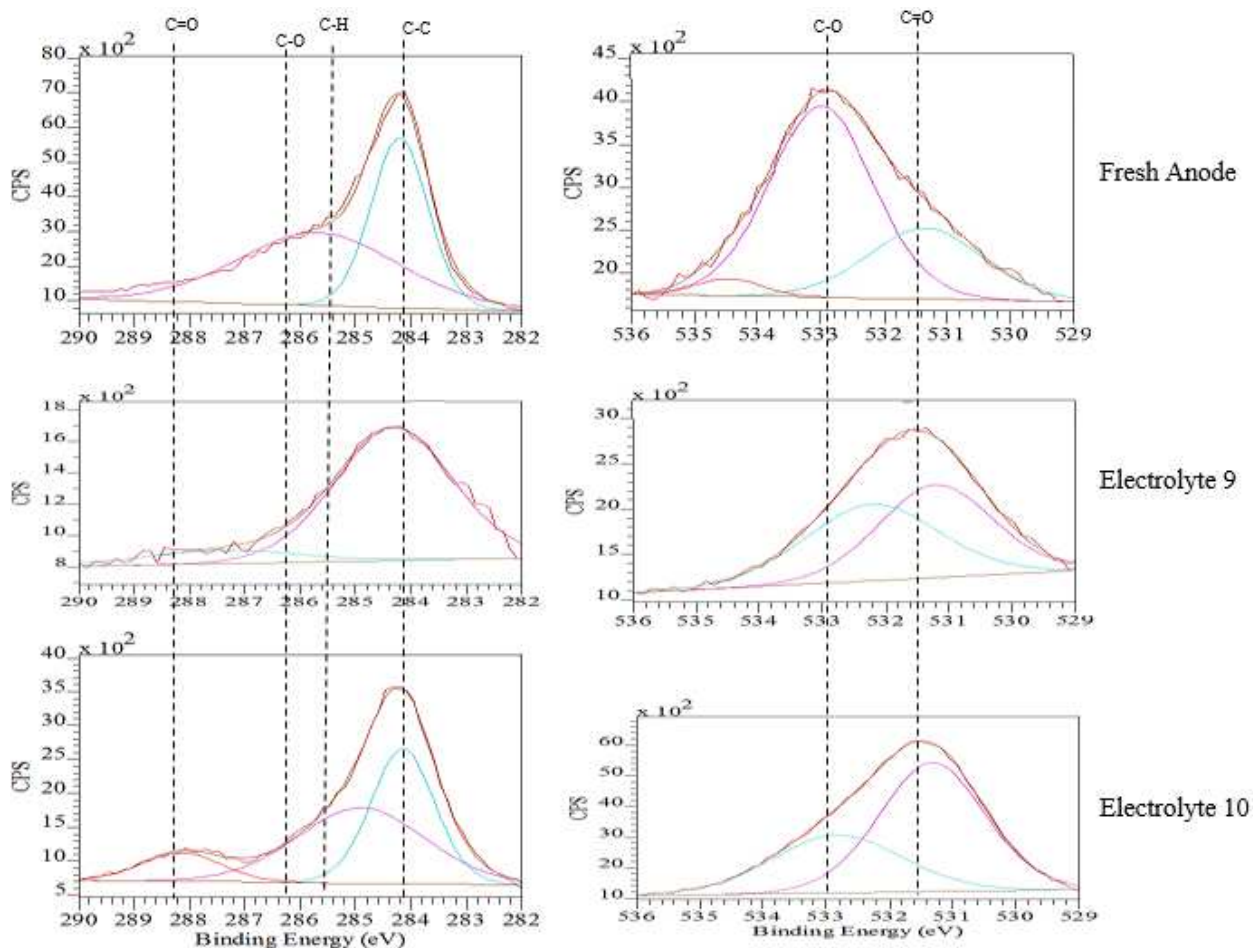


Figure 25. C1s (left) and O1s (right) XPS spectra of anodes cycled for 200 cycles at 60°C .

Compared to the fresh anode surface, the cycled anode had quite a different spectra. This proved that the anode surface was completely covered with an SEI layer. The C1s peak at 284.3 eV showed the presence of C-C and the peak at 285.7 eV corresponds to C-H species. The peaks at 286-287 eV and 288-289 eV corresponded to C-O and C=O species, respectively [50]. The C1s peaks for electrolyte 9 were considerably diminished. Similarly, the O1s spectra for electrolyte 9 showed that there was bigger peak for C-O (531-532 eV) but the C=O peak (533 eV) was reduced. The C=O species (288- 289 eV) was also very small in C1s spectra.

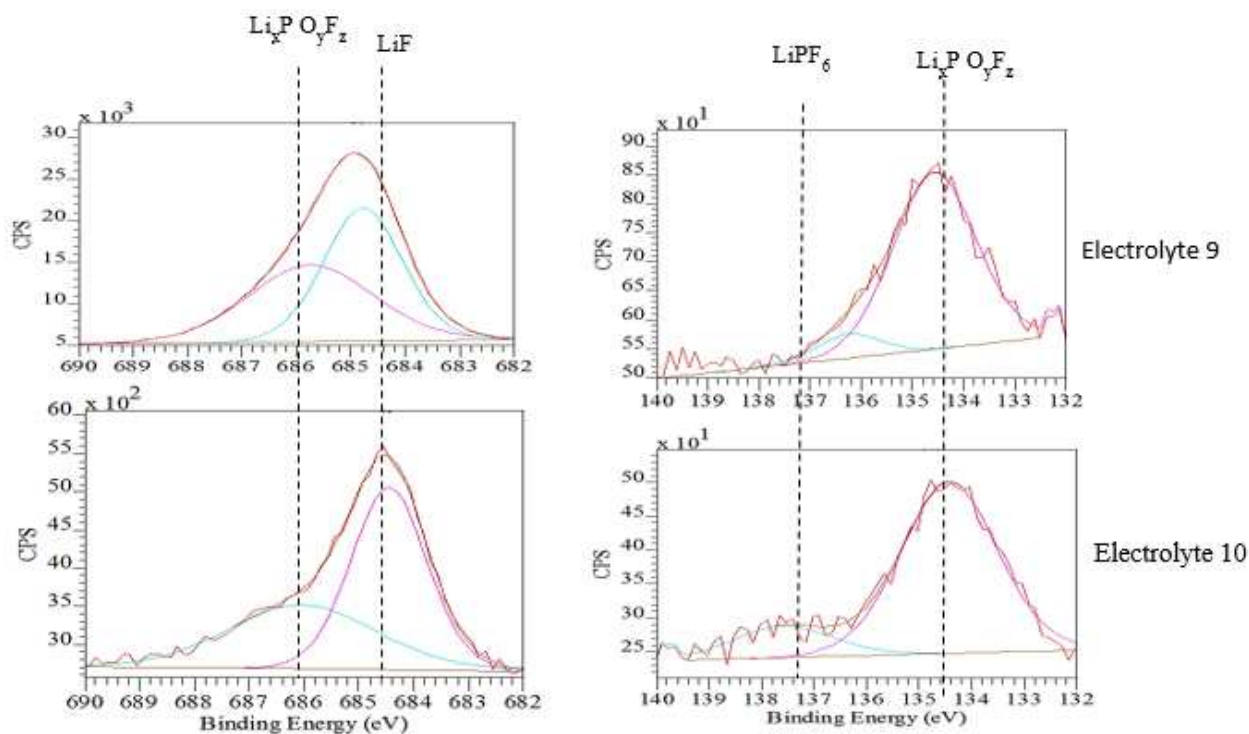


Figure 26. F1s (left) and P2p (right) XPS spectra of anodes cycles for 200 cycles at 60°C.

Figure 26 shows the F1s and P2p spectra of the anodes cycled with electrolyte 9 and electrolyte 10. The peak at 684 – 685 eV in F1s spectra represented a LiF compound. The peak at 686 eV – 687 eV was from $\text{Li}_x\text{PO}_y\text{F}_z$ species. In the P2p spectra, the peak at 134 eV – 135 eV also corresponds to $\text{Li}_x\text{PO}_y\text{F}_z$ species [50].

Table 10 compares the elemental concentrations in the SEI layer derived from the spectra discussed above for different electrolyte systems. The carbon and oxygen elemental percentage were very similar (more than 50 %) for both 10 and 12. However, the carbon and oxygen concentrations were low for electrolyte 9 (15.5 and 9.6 percent). In addition, there was not much of a difference in phosphorus concentration.

Table 10. Elemental concentration on anode for different electrolytes

| Electrolytes | Surface elemental concentration (%) on the anode surface | | | |
|--------------------|--|------|------|-----|
| | C | O | F | P |
| Fresh anode | 83.6 | 16.6 | | |
| 10 | 57.8 | 28 | 10.5 | 3.7 |
| 9 | 15.5 | 9.6 | 70.6 | 4.1 |
| 12 | 54.6 | 24.8 | 16.2 | 4.3 |

A stark difference in the fluorine concentration can be observed. Electrolyte 9 was found to have its SEI layer composed of 70% fluorine, while electrolytes 10 and 12 gave only 10 and 16 percent, respectively. It appears that the SEI layer containing LiF species had less resistivity.

Extending this thought unto the other electrolytes containing VC and LiBOB as additive, there is a clear trend as seen in Figure 27. As fluorine species (F1s) increases, performance at low temperature also increases. The opposite effect occurs with carbon species (C1s), as when it reduces, there is a detrimental effect on low temperature capacity. This impact however, is not as prominent when in comparison to -20°C performance. Table 11 outlines the amount of each species for all electrolyte combinations tested.

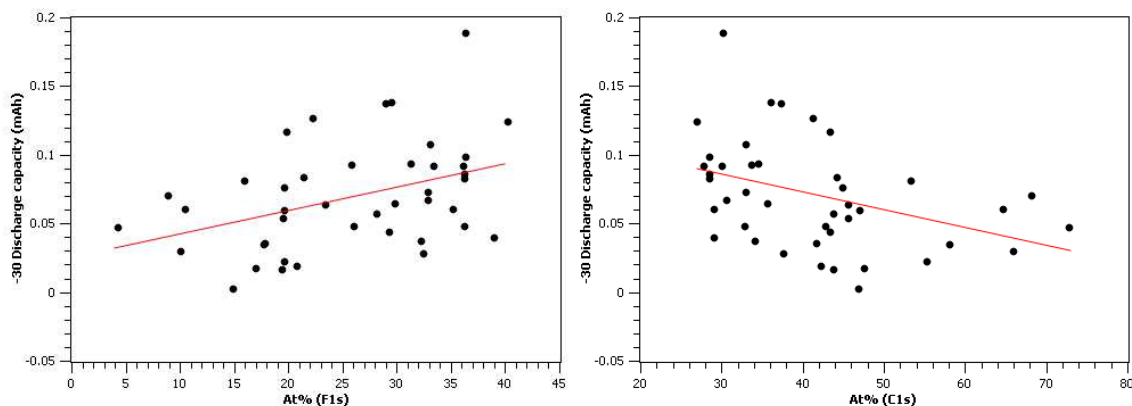


Figure 27. F1s (left) and C1s (right) graphs of discharge capacity (5C rate) vs. elemental concentration at -30°C.

Table 11. Elemental concentration on anode for electrolytes with VC and LiBOB additive

| Electrolytes | Surface elemental concentration (%) on the anode surface | | | |
|--------------------|--|-------|-------|------|
| | C | O | F | P |
| Fresh anode | 83.6 | 16.6 | | |
| 1 | 46.87 | 35.99 | 14.89 | 2.24 |
| 2 | 29.05 | 27.98 | 39.04 | 3.92 |
| 3 | 32.96 | 26.09 | 36.27 | 4.68 |
| 4 | 30.26 | 28.58 | 36.43 | 4.73 |
| 5 | 37.71 | 26.43 | 32.49 | 3.38 |
| 6 | 45.72 | 27.13 | 23.46 | 3.70 |
| 7 | 45.66 | 30.51 | 19.57 | 4.25 |
| 8 | 36.08 | 29.63 | 29.56 | 4.72 |
| 9 | 15.50 | 9.60 | 70.60 | 4.10 |
| 10 | 57.80 | 28.00 | 10.50 | 3.70 |
| 14 | 44.25 | 30.06 | 21.46 | 4.22 |
| 15 | 47.05 | 29.72 | 19.62 | 3.61 |
| 16 | 43.80 | 32.09 | 19.40 | 4.70 |
| 17 | 34.22 | 26.71 | 32.29 | 6.79 |
| 18 | 27.04 | 27.88 | 40.31 | 4.77 |
| 19 | 53.35 | 28.46 | 15.95 | 2.24 |
| 20 | 30.09 | 30.83 | 33.46 | 5.61 |
| 21 | 42.88 | 25.75 | 26.12 | 5.25 |
| 22 | 37.38 | 29.57 | 29.04 | 4.01 |
| 23 | 33.00 | 29.01 | 33.16 | 4.84 |
| 24 | 64.65 | 22.76 | 10.52 | 2.08 |
| 25 | 44.94 | 32.19 | 19.63 | 3.24 |
| 26 | 42.34 | 31.39 | 20.84 | 5.43 |

| | | | | |
|-----------|-------|-------|-------|------|
| 27 | 28.57 | 29.83 | 36.27 | 5.33 |
| 28 | 33.04 | 29.56 | 32.93 | 4.48 |
| 29 | 43.89 | 24.19 | 28.14 | 3.78 |
| 30 | 29.11 | 30.86 | 35.25 | 4.78 |
| 31 | 41.74 | 33.96 | 17.84 | 6.47 |
| 32 | 68.23 | 21.98 | 8.95 | 0.84 |
| 33 | 72.90 | 22.77 | 4.32 | 0.00 |
| 34 | 47.64 | 30.92 | 17.04 | 4.40 |
| 35 | 41.28 | 33.27 | 22.31 | 3.14 |
| 36 | 43.36 | 32.92 | 19.87 | 3.84 |
| 37 | 66.04 | 21.76 | 10.12 | 2.09 |
| 38 | 34.55 | 29.33 | 31.34 | 4.78 |
| 39 | 58.19 | 21.57 | 17.73 | 2.51 |
| 40 | 35.77 | 27.64 | 29.83 | 6.77 |
| 41 | 33.69 | 35.75 | 25.91 | 4.65 |
| 42 | 27.91 | 30.62 | 36.15 | 5.32 |
| 43 | 55.27 | 21.98 | 19.62 | 3.13 |
| 44 | 43.46 | 23.63 | 29.35 | 3.56 |
| 45 | 28.52 | 29.76 | 36.40 | 5.32 |
| 46 | 28.58 | 29.62 | 36.23 | 5.57 |

When looking at particular component species within both the C1s and F1s spectra, there seems to be the effect of both LiF and $\text{Li}_x\text{PO}_y\text{F}_z$ bonds for the F1s spectra. In addition, the C-H bond as evidenced in Figure 28 seems to show the opposite effect of F1s. As LiF and $\text{Li}_x\text{PO}_y\text{F}_z$ concentration increases, low temperature capacity also increases. As C-O concentration increases, lower temperature capacity decreases. This is similarly seen with other C1s bonds, however, not to the same degree.

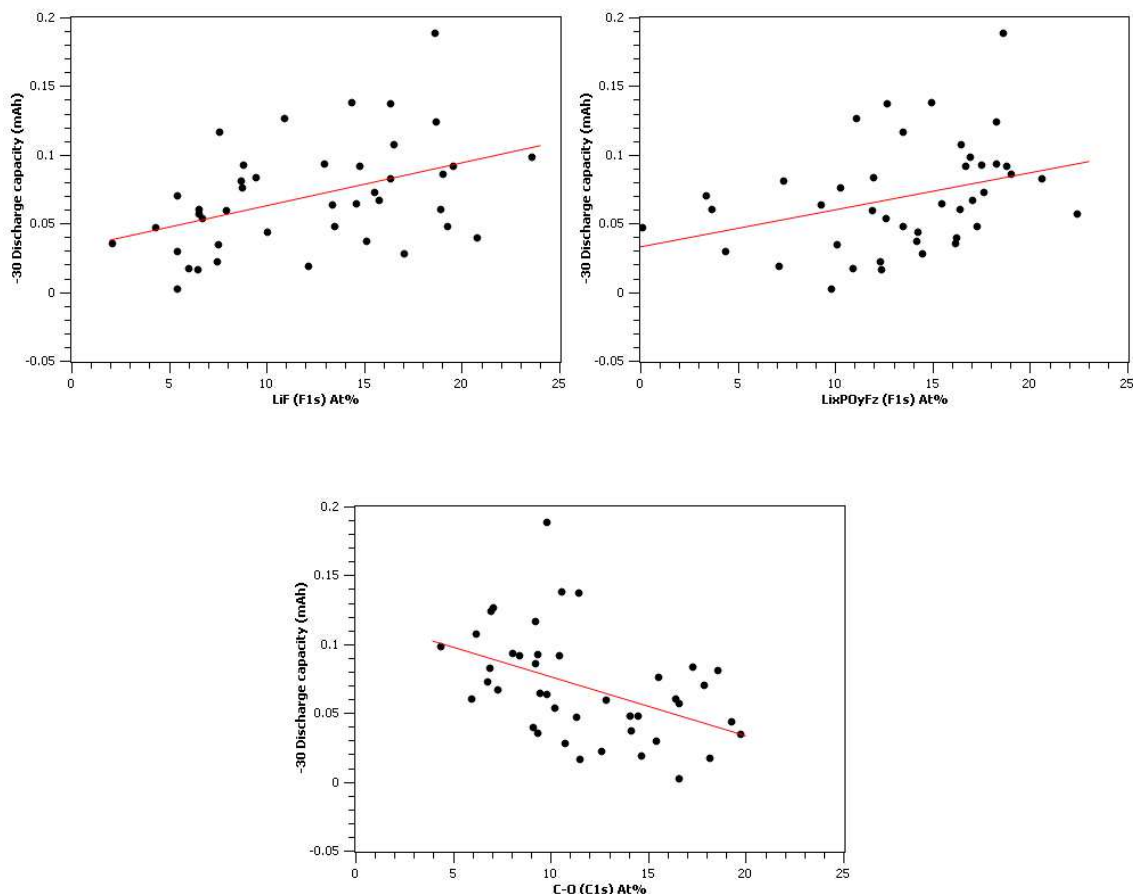


Figure 28. LiF (left), $\text{Li}_x\text{PO}_y\text{F}_z$ (right), and C-O (bottom) graphs of discharge capacity (5C rate) vs. elemental concentration at -30°C .

3.3 ELECTROCHEMICAL IMPEDANCE

After the formation cycles, the surface of the LIB graphite anode is covered by the SEI layer, which prevent the further chemical or electrochemical reactions between the electrolyte and the carbon anode. The SEI layer has a porous physical structure, the density of this porous structure is critical for performance of anode. The reactions between electrode and electrolyte cannot be effectively prevented if the SEI layer is too porous, while if it is too dense, it can negatively impact the power of the anode. Figure 29 shows a comparison of the impedance spectra

for anode in electrolytes 12, 13, Cs, and 9 at 25°C. As shown previously, electrolyte 12 has good low temperature performance at -20°C with 0.63 mAh, which was an improvement as it had VC additive over electrolyte 11. Electrolyte 13 had only EMC solvent comprised in the electrolyte and showed very good results at -20°C and -30°C at 0.74 mAh and 0.39 mAh, respectively. Electrolyte 9 also did very well at -20°C (0.74 mAh) and -30°C (0.35 mAh) low temperature performance, where the electrolyte had all solvent components except for DEC. Lastly, Cs additive electrolyte was tested for comparison purposes as it was previously reported to have good low temperature performance [49]. However, Cs additive electrolyte did not show as good a performance as other electrolytes above showing only 0.41 mAh and 0.11 mAh discharge capacity at -20°C and -30°C, respectively. The equivalent circuit used for the numerical fitting is shown as inset in the figure. Also the enlarged high frequency semi-circle is also shown as an inset. In the equivalent circuit, R_s represents ohmic resistance which could be a result of the material's intrinsic resistance and the contact resistance in the cell; the R/C component represents the SEI layer where C_{pseudo} is the possible pseudo capacitance while R is the diffusion resistance of a Li-ion across the SEI layer. The CPE is a constant phase element which used to simulate the distributed network of double layer capacitance and resistance in a porous electrode, here $CPE_{\text{SEI}}/R_{\text{ctSEI}}$ is used to simulate the possible side reactions between electrode and electrolyte. The last CPE_e/R_{cte} component, of course, represents the charge transfer and Li-ion insertion reaction at the

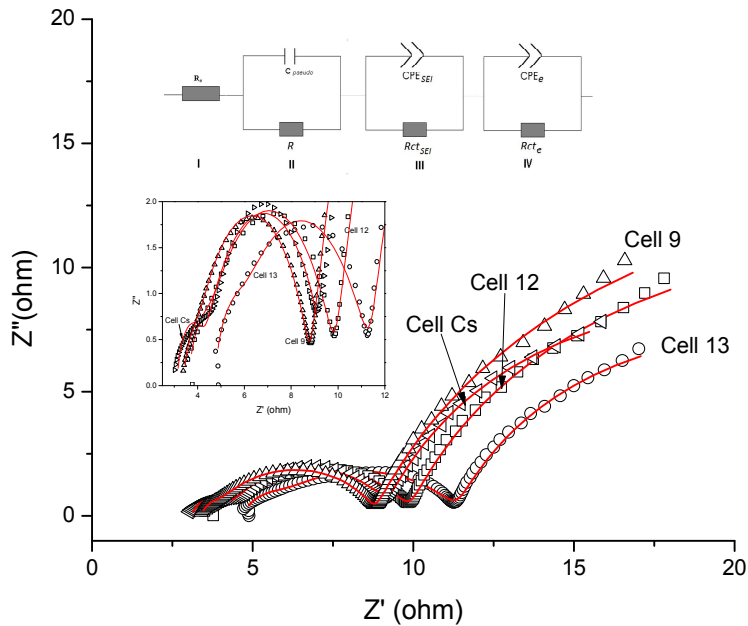


Figure 29. ac-impedance and fitting for fresh cells (after formation) at 25°C. The insets show the equivalent circuit used in the fitting and the enlargement of high frequency portion of the impedance spectra.

interface of the electrode and SEI layer. Clearly, the equivalent circuit fitted the experimental data well. The equivalent circuit for fitting the impedance spectra obtained at low temperature (-20°C) can be simplified. In figure 30, the equivalent circuit is shown as an inset. The difference was that the CPE_{SEI}/R_{ctSEI} was not needed. Excellent fitting is shown in the figure. The fitting results are tabulated in Table 12. It is worth to discussing the difference between the C_{pseudo}/R loop and the CPE_{SEI}/R_{SEI} loop. They were both used to simulate the SEI layer. However, the former was used to simulate the Li-ion mass transfer through the SEI layer in which C_{pseudo} represented the “capacitor-like” or “pseudo capacitor” behavior resulted from the non-homogeneous or even porous nature of the SEI layer,

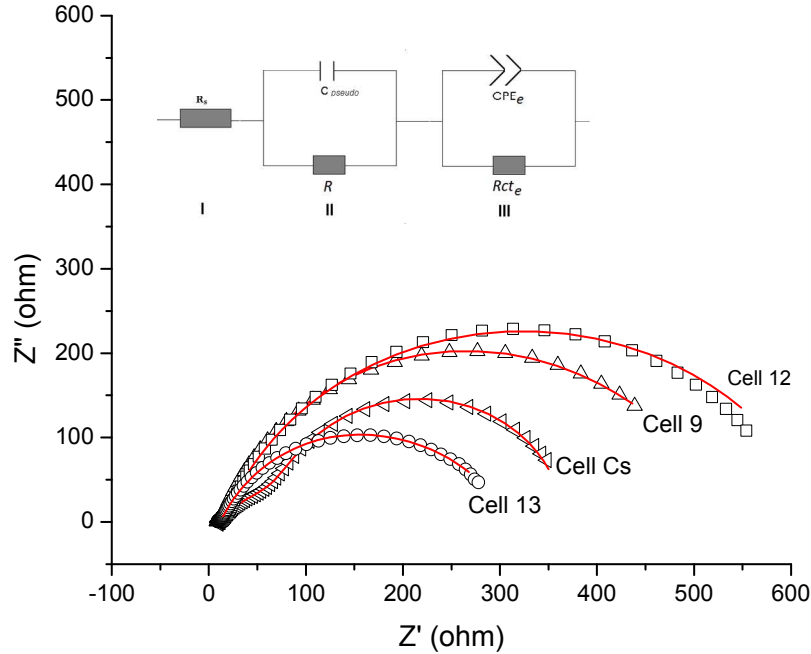


Figure 30. ac-impedance and fitting for fresh cells (after formation) at -20°C. The inset shows the equivalent circuit used in the fitting.

while R represented the diffusion resistance. The CPE is used to model the distributed capacitor – resistor network for a non-homogeneous matrix. When CPE-P is equal to 0.5, then the CPE becomes an infinite length Warburg element which demonstrates a homogenous charge diffusion, the well-known 45 degree line will be shown on the Complex-Plane graph. The deviation of CPE-P from 0.5 illustrates the degree the system deviates from homogeneity. CPE-T is a time parameter, mathematically, when CPE-E=0.5, $1/\text{CPE-T}$ is proportional to the diffusion coefficient. Therefore, a CPE/R loop was used to simulate an electrochemical charge transfer reaction in a diffused, non-homogeneous and porous matrix. In this report, $\text{CPE}_{\text{SEI}}/R$ and CPE_e/R_e stood for the possible side reaction e.g. small decomposition of electrolyte and Li insertion reaction on the carbon electrode, respectively. According to the fitting of the impedance spectra (shown in figure 29 and 30) there remains residual electrochemical decomposition of electrolyte at room temperature but the reaction

can be ignored at -20°C . It is reasonable to assume that the rate for the decomposition of electrolyte was low, otherwise, the cell would not cycle well. Thus, the larger semi-circle in figure 29 at low frequency was attributed to side reactions, while the higher frequency semi-circle resulted from the charge transfer reaction at carbon/SEI interface and the subsequent insertion into the carbon structure.

As illustrated in Table 12, the Ohmic resistance (R_s) increased substantially when the temperature changed from 25°C to -20°C , however R_s for the different cells were almost all the same at the corresponding temperature, which shows not only the excellent cell engineering and reproducibility, but also that the conductivity of the electrolyte may contribute little to the differences in the cell performance. When the cells were fresh (after formation before duty cycles), the C_{pseudo} and R were almost the same at 25°C , which shows that a similar SEI layer was formed. At -20°C , the C_{pseudo} and R for 9, 13, and Cs cells similarly changed with the same trend, the values of both parameters increased. The detailed analysis of the fitting data can reveal something interesting regarding the SEI layer formed on the anodes in the three cells. The $\text{CPE}_{\text{SEI-P}}$ for cells 13 and Cs (0.82 and 0.84, respectively) deviated away from 0.5 more than that of cell 9 (0.78), which demonstrated the more non-homogenous nature of the SEI layers in cell 13 and Cs. The same trend was seen in the change of C_{pseudo} for cell 13 and Cs, which was more than two times as that of cell 9.

Table 13 shows the discharge capacity of those cells after one thermo-cycle (60°C , 100 cycles). Evidently, cell 9 survived the thermo-cycle much better. It seems that the non-homogeneous and/or porous SEI layer did not survive the thermo-cycle well, especially the low temperature performance after thermo-cycles. Cell 12 seemed to be an outlier, but it is worth pointing out that the $\text{CPE}_{\text{SEI-P}}$ at 25°C for the cell was at the same level as that of cells 13 and Cs,

the non-homogeneous SEI layer went through a significant change at -20°C. The morphology change of the SEI layer made the Li diffusion resistance (R) of cell 12 the lowest one among the four. However, such alteration substantially increased the charge transfer resistance (R_{ct}) for the Li-ion insertion process. The net effect makes cell 12 a low performer at -20°C. In addition, cell 12 suffered during thermo-cycling due to the non-homogenous SEI layer. R_{ctSEI} values for the four cells provided additional evidence to prove the hypothesis that the SEI layer in cell 9 was more stable. Among all the R_{ctSEI} s, which represented the resistance of electrochemical decomposition of electrolyte, R_{ctSEI} for cell 9 was the highest.

CPE_e-T , CPE_e-P , and R_e simulated the charge transfer Li insertion reaction. It should be emphasized that the electrochemical reaction occurred at the interface between the carbon anode and SEI layer, in which the electrochemical decomposition of electrolyte also took place. However, they were in the different time domains. The most notable aspects were the exceptionally high charge transfer resistance (R_{ct}) and low R_e for cell Cs. The latter one may due to the catalytic effect of Cs additive in the electrolyte.

Table 12. Equivalent fitting results for the impedance spectra shown in figure 29 and 30

| | Temp(°C) | $R_s(\Omega)$ | C_{pseudo} (mF) | $R(\Omega)$ | CPE_{SEI-T} T x10 ³ | CPE_{SEI-P} P | R_{ctSEI} (Ω) | CPE_{e-T} T | CPE_{e-P} P | R_{cte} (Ω) |
|-----------|----------|---------------|----------------------|-------------|-------------------------------------|--------------------|-----------------------------|------------------|------------------|---------------------------|
| 12 | 25 | 3.6 | 0.12 | 0.68 | 0.52 | 0.81 | 28.2 | 2.0 | 0.75 | 5.6 |
| 12 | -20 | 11.5 | 0.035 | 4.16 | - | - | - | 0.61 | 0.81 | 616.9 |
| 13 | 25 | 4.7 | 0.12 | 0.81 | 0.59 | 0.82 | 19.1 | 2.9 | 0.68 | 5.9 |
| 13 | -20 | 11.82 | 2.4 | 38.73 | - | - | - | 0.90 | 0.74 | 259.3 |
| 9 | 25 | 3.4 | 0.19 | 0.5 | 0.5 | 0.78 | 34.5 | 1.3 | 0.81 | 4.9 |

| | | | | | | | | | | |
|-----------|-----|-------|------|-------|-----|------|-------|-----|------|-------|
| 9 | -20 | 10.48 | 1.1 | 176.4 | - | - | - | 1.1 | 0.74 | 352.8 |
| Cs | 25 | 3.1 | 0.16 | 1.1 | 0.7 | 0.84 | 21.52 | 6.4 | 0.81 | 4.9 |
| Cs | -20 | 12.9 | 4.1 | 278 | - | - | - | 1.8 | 0.68 | 74.3 |

Table 13. Low temperature performance for the cells after thermo-cycle at 60°C for 100 cycles.

| Electrolyte | Discharge Capacity at 25°C (mAh) | Discharge Capacity at -20°C (mAh) | Discharge Capacity at -30°C (mAh) |
|--------------------|---|--|--|
| 13 | 0.88 | 0.50 | 0.05 |
| 12 | 0.82 | 0.32 | 0.02 |
| 9 | 1.05 | 0.67 | 0.18 |
| Cs | 0.87 | 0.20 | 0.08 |

In summary, it has been found that a high concentration of EMC and DMC were required to increase the low temperature performance of the cells. DMC solvent is slightly favored over EMC. High concentration of PC and EC are unfavorable for low temperature performance but their presence is found to be essential for the stability of SEI at high temperatures.

3.4 X-RAY DIFFRACTION (XRD)

Results from XRD method are seen in Figure 31 for representative electrolytes 1-10 with analysis of 2θ values from 20° to 90° . In order to remove the possible error in comparing between different spectra obtained, relative intensities of the diffraction peaks was calculated instead of absolute intensities. This was done by dividing the absolute intensity of every peak by the absolute intensity of the most intense peak, which is then converted to a percentage. The most intense peak would thus be at 100% for each spectra obtained. Electrolytes shown were stacked in the figure as to not have one on top of each other. Fresh uncycled anode was analyzed as seen in Figure 32 and 33 for phase identification. The first material that had best peak fitting was from copper with pattern number cod 7101264, which correlates to the substrate used to coat the anode material. Planes identified include (1,1,1), (2,0,0), (2,2,0), and (3,1,1) for the Cu material. The relative intensities corresponding to these planes are 12.30%, 4.96%, 15.82%, and 4.08%, respectively. Table 14 also outlines the planes corresponding to the relative intensity and d_{hkl} .

The second material identified for the anode that fit the XRD Spectra was graphite with pattern number cod 9012230, which correlates to the active material used for the anode electrode. Planes identified with the peaks include (0,0,2) and (0,0,4) with relative intensities at 100% and 3.96%, respectively. Table 15 also outlines the planes corresponding to the relative intensity and d_{hkl} .

The peaks for Cu material matched with the database, however, this was not seen with peaks identified in the database for graphite material. Some of the missing planes include (1,0,0), (1,0,1), (1,0,2), (1,0,3), (1,0,4), (2,1,0), (2,1,2), (1,0,5), (0,0,6). Possible factors that may contribute to differences seen in the peak profile could be scanning setup, crystallite size,

microstrain, inhomogeneity, impurities, and errors in sample preparation or setup. If the plane normal is not parallel to the diffraction vector, a diffraction peak will not be produced and only background is observed. Electrolyte 5 also seem to have an issue with its analysis as the peaks and background shifted roughly 5% higher in relative intensity.

When looking closer at 2θ value of around 26° , which correlates to the carbon in graphene sheets, there seems to be slight shifts in the spectrum as seen in Figure 34. The largest shift versus fresh anode comes from electrolyte 9 and 10, which moved from $\sim 26.1^\circ$ peak to 26.4° peak. In a study done by Whitehead et al., they found that the XRD patterns shifted from the (002) peak for graphite electrode signifying structural changes that occur during various degrees of lithium intercalation [56]. However, when comparing the performance of electrolyte 9 and electrolyte 10, they had a performance of 0.74 and 0.53 mAh at -20°C , respectively. This shift however, is not seen at the same degree for other electrolytes that also did very well (>0.50 mAh) at -20°C , which were electrolytes 4, 6, and 8.

Unfortunately, XRD technique did not show anything conclusive as far as any differences between good and bad performing electrolytes at low temperature.

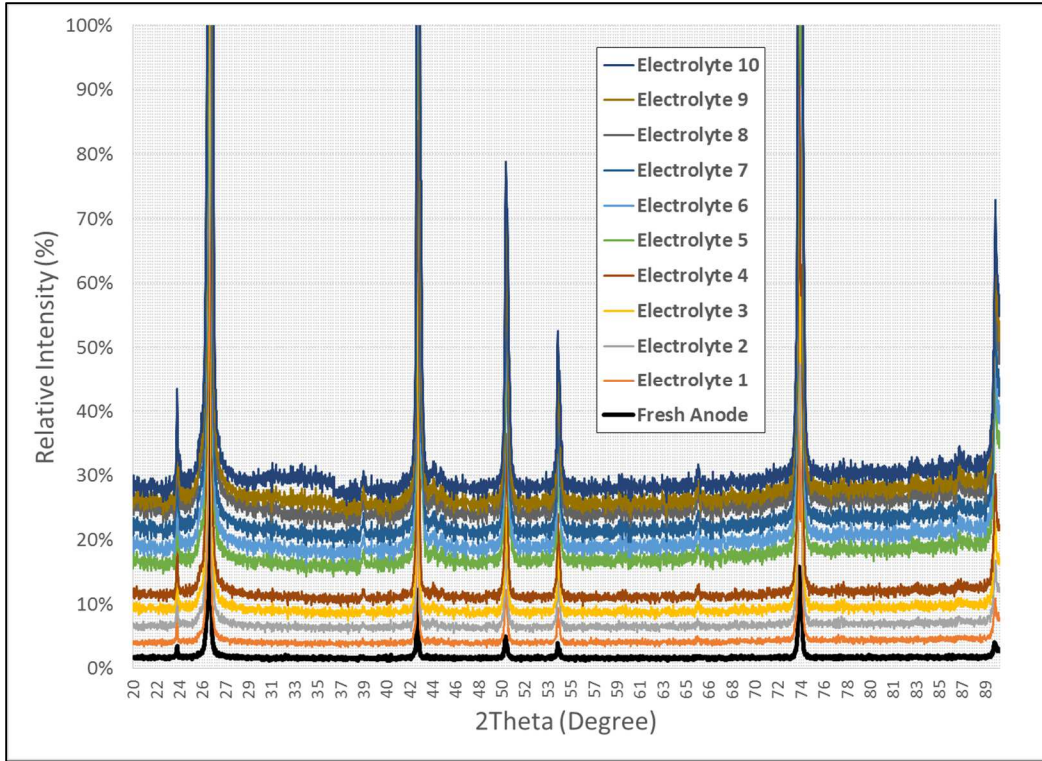


Figure 31. XRD spectra of different electrolyte compositions

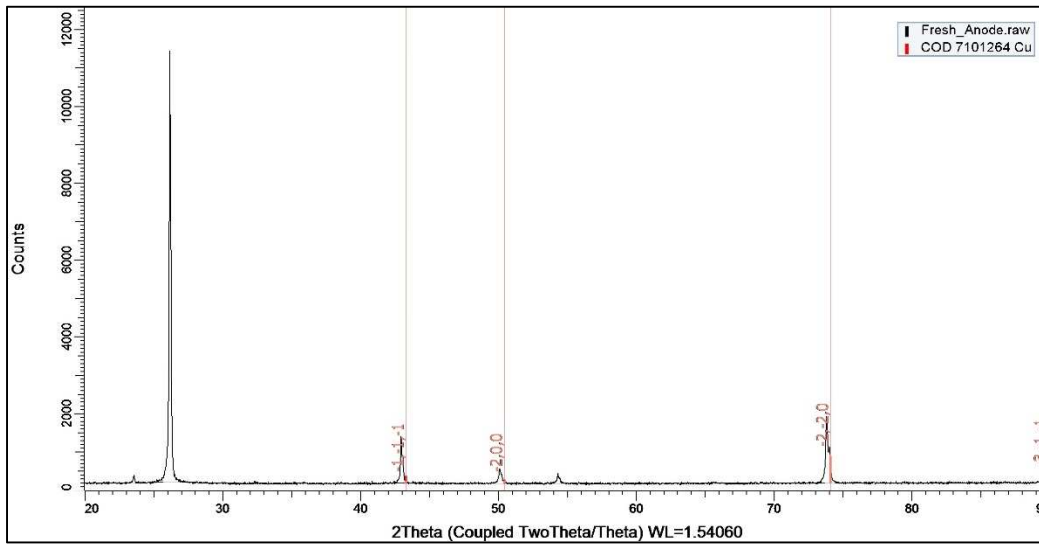


Figure 32. Plane Identification of Fresh Anode (Cu)

Table 14. Relative Intensities of Fresh Anode (Cu)

| Plane | d_{hkl} (Å) | Relative Density (%) |
|-------|------------------|----------------------------|
| (111) | 2.104564 | 12.30% |
| (200) | 1.819281 | 4.96% |
| (220) | 1.282935 | 15.82% |
| (311) | 1.092999 | 4.08% |

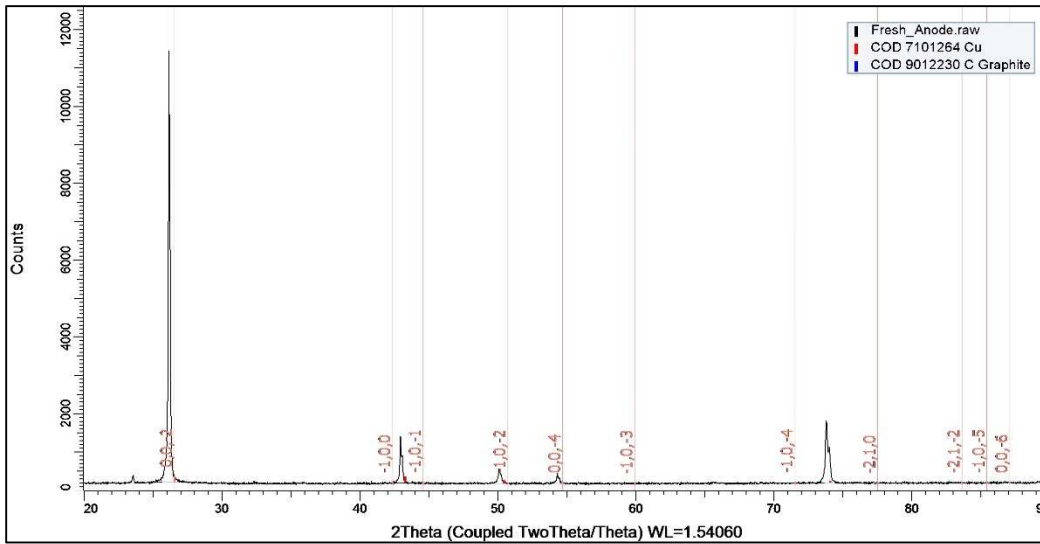


Figure 33. Plane Identification of Fresh Anode (Graphite)

Table 15. Relative Intensities of Fresh Anode (Graphite)

| Plane | d_{hkl} (Å) | Relative Density (%) |
|-------|------------------|----------------------------|
| (002) | 3.403719 | 100.00% |
| (004) | 1.687490 | 3.96% |

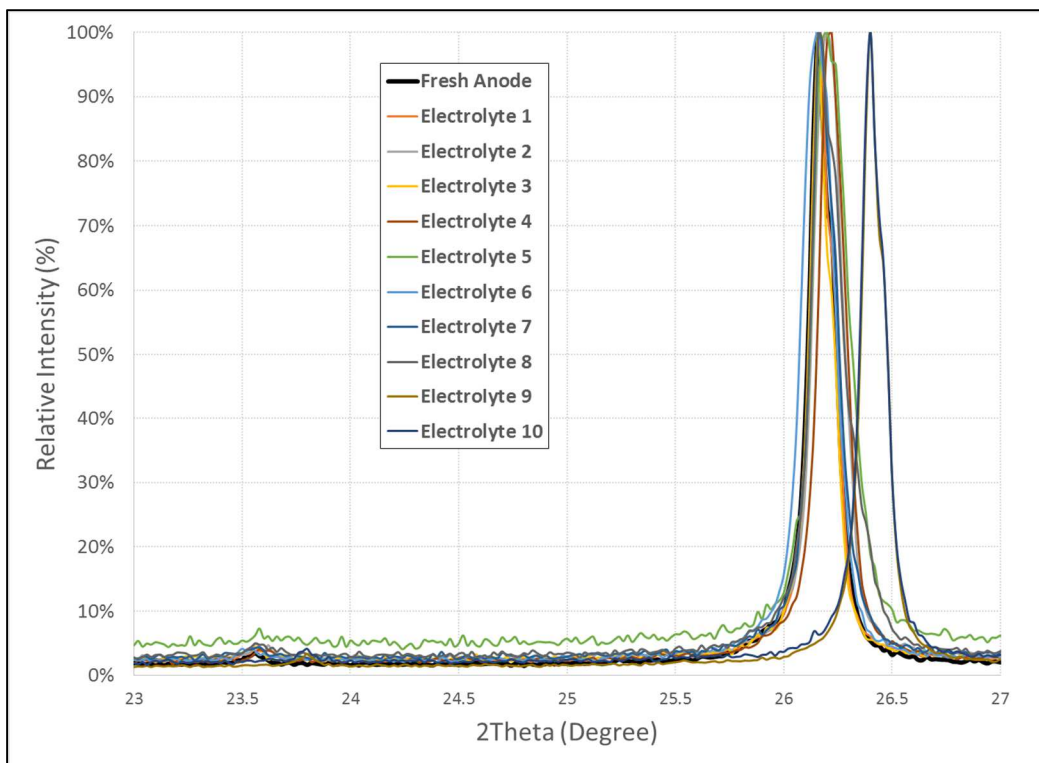


Figure 34. XRD spectra of Graphite at 2θ of $\sim 26^\circ$ for different electrolyte compositions

CHAPTER 4 – ANALYSIS AND DISCUSSION

4.1 CONCLUSIONS

Many different combinations of solvent compositions were studied for LIB electrolyte in a low temperature application (keeping LiPF_6 and additive concentrations constant). Through systematic variations of solvent types, we are able to see the impact of cell performance at wide range of temperatures. Our results show that solvent selection can make a significant impact on the SEI formation, and consequently on the battery performance. The electrochemical impedance and fitting revealed that the homogeneity of the SEI layer and its catalytic aspect on the carbon interface played a large role. The low temperature performance depended more on the SEI quality than the conductivity of the solvent. The low percentage of cyclic carbonates and high percentage of short chain linear carbonates favored the low temperature performance based on electrical testing. However, some cyclic carbonates were necessary to retain the cell performance at elevated temperature. For instance, the addition of VC improved the -20C discharge performance from 0.50 mAh to 0.63 mAh, as evidenced in electrolytes 11 and 12. Based on performances from all 43 electrolytes from the DOE, decreasing the cyclic carbonates EC and PC from 60% to 25% improved the -20C performance from 0.1 mAh to roughly 0.65 mAh, showing a 550% improvement. Additionally, increasing the short linear carbonates improved the -20C performance from 0.15 mAh to 0.60 mAh, showing a 300% improvement. Electrolyte 9 is a good representation of this as it had the lowest amount of cyclic carbonates at 25% (20% EC and 5% PC due to DOE boundaries set) with higher short linear carbonates at 75%. XPS analysis of cycled electrodes show that the better performing electrolytes give higher percentages of LiF in SEI whereas bad performing electrolytes gives more carbon containing species. Most importantly, we demonstrated that the low temperature power capability of an LIB

can be substantially improved not by adding exotic additives into the electrolyte, but by rational design of the composition of the most commonly used solvents.

4.2 FUTURE WORK

Even with many advancements in Li-ion batteries as of late, there are still many improvements to be made. Especially for vehicle applications, many hurdles such as improvements in wide temperature operation, long cycle life, rate performance, energy densities, power densities, among others, leave much to be desired.

Not only can slight electrolyte modifications improve performance in these applications as seen in this study, but changes in the cathode material, anode material, and other components that are comprised in a lithium-ion battery can be made to overcome issues seen today. Improvements in cathode materials may include additives and/or coatings to improve conductivity and performance, or changes such as particle surface modification and compositions. However, even with material changes that are made in a lithium-ion battery, a suitable electrolyte will also need to be considered as current electrolytes systems are tailor-made for the specific cell chemistry. This is of much importance as the electrolyte components yield certain surface chemistries on metal oxide cathodes and especially on graphitic anodes.

Through our findings with various compositions of different carbonates, we can investigate further by fine-tuning the boundaries of each component. As mentioned previously, EC was fixed between 20-30%, PC between 5-30%, EMC at 0-70%, DMC at 0-40%, and DEC at 0-40%. From what we have learned on how each component effects both low and high temperature performance, a possible next round of investigations would be to lower both EC and PC cyclic carbonates and increasing EMC and DMC short linear carbonates. Table 16 below shows the next round of

investigations that would hone in on the issues with wide temperature electrolytes without using novel electrolyte components.

Table 16. Future work on electrolyte compositions

| Electrolyte Bounds | | |
|--------------------|-------|-------|
| Component | Lower | Upper |
| EC | 5 | 25 |
| PC | 0 | 10 |
| EMC | 30 | 70 |
| DMC | 30 | 70 |
| DEC | 0 | 0 |

REFERENCES

1. Lowe, M.; Tokuoka, S.; Trigg, T.; Gereffi, G., 2010, Lithium-ion batteries for hybrid and all-electric Vehicles: the U.S. Value Chain, Center on Globalization, Governance & Competitiveness, Duke University, p. 1-76.
2. Xu, K., 2004, Nonaqueous liquid electrolytes for lithium-based rechargeable batteries, *Chem. Rev.*, 104, p. 4303-4417.
3. Linden, B.; Reddy, T., 2001, *Linden's Handbook of Batteries*, McGraw-Hill, p 1.3-15.3.
4. Jasinski, R., 1967, *High energy batteries*, Plenum Press, New York
5. Whittingham, M. S., 1976, Electrical energy storage and intercalation chemistry, *Science*, 192, p. 1126.
6. Whittingham, M. S., 1978, Chemistry of intercalation compounds: metal guests in chalcogenide hosts, *Prog. Solid State Chem.*, 12, 1, p. 41-99.
7. Mizushima, K.; Jones, P. C.; Wiseman, P. J.; Goodenough, J. B., 1981, Li_xCoO_2 ($0 < x \leq 1$): A new cathode material for batteries of high energy density, *Solid State Ionics*, 3/ 4, 171.
8. Murphy, D.W.; Christian, P.A., 1979, Solid state electrodes for high energy batteries, *P. Science*, 205, 651.
9. Nagaura, T.; Nagamine, M.; Tanabe, I.; Miyamoto, N., 1989, *Prog. Batteries Sol. Cells*, 8, 84.
10. Nagaura, T.; Ozawa, K., 1990, *Prog. Batteries Sol. Cells*, 9, 209.
11. Nishi, Y.; Azuma, H.; Omaru, A., 1990, U.S. Patent 4, 959, 281.
12. Fong, R.; von Sacken, U.; Dahn, J. R., 1990, Studies of lithium intercalation into carbons using nonaqueous electrochemical cells, *J. Electrochem. Soc.*, 137, 7, p. 2009.
13. Nie, M.; Abraham, D.; Seo, D.; Chen, Y.; Bose, A.; Brett., L., 2013, Role of solution structure in solid electrolyte interphase formation on graphite with LiPF_6 in propylene carbonate, *J. Phys. Chem. C*, 117, p. 25381–25389.
14. Herstedt, M.; Andersson, A. M.; Rensmo, H.; Siegbahn, H.; Edström, K., 2004, Characterization of the SEI formed on natural graphite in PC-based electrolytes, *Electrochim. Acta*, 49, p. 4939–4947.

15. Inaba, M.; Siroma, Z.; Kawatate, Y.; Funabiki, A.; Ogumi, Z., 1997, Electrochemical scanning tunneling microscopy analysis of the surface reactions on graphite basal plane in ethylene carbonate-based solvents and propylene carbonate, *J. Power Sources*, 68, p. 221–226.
16. Jeong, S.-K.; Inaba, M.; Iriyama, Y.; Abe, T.; Ogumi, Z., 2003, AFM study of surface film formation on a composite graphite electrode in lithium-ion batteries, *J. Power Sources*, 119–121, p. 555–560.
17. Chung, G.C.; Kim, H.J.; Yu, S.I.; Jun, S.H.; Choi, J.W.; Kim, M.H., 2000, Origin of graphite exfoliation an investigation of the important role of solvent cointercalation, *J. Electrochem. Soc.*, 147, p. 4391–4398.
18. Wang, J.; Manga, K.K.; Bao, Q.; Loh, K.P., 2011, High-Yield synthesis of few-layer graphene flakes through electrochemical expansion of graphite in propylene carbonate electrolyte, *J. Am. Chem. Soc.*, 133, p. 8888–8891.
19. Tasaki, K., 2005, Solvent decompositions and physical properties of decomposition compounds in li-ion battery electrolytes studied by DFT calculations and molecular dynamics simulations, *J. Phys. Chem. B*, 109, p. 2920–2933.
20. Aurbach, D.; Daroux, M.L.; Faguy, P.W.; Yeager, E., 1987, Identification of surface films formed on lithium in propylene carbonate solutions, *J. Electrochem. Soc.*, 134, 1611–1620.
21. Pistoia, G.; De Rossi, M.; Scrosati, B., 1970, *J. Electrochem. Soc.*, 117, 500.
22. Guyomard, D.; Tarascon, J.M., 1993, Rechargeable $\text{Li}_{1+x}\text{Mn}_2\text{O}_4$ / Carbon cells with a new electrolyte composition potentiostatic studies and application to practical cells, *J. Electrochem. Soc.*, 140, p. 3071.
23. Tarascon, J. M.; Guyomard, D., 1994, New electrolyte compositions stable over the 0 to 5 V voltage range and compatible with the $\text{Li}_{1+x}\text{Mn}_2\text{O}_4$ /carbon Li-ion cells, *Solid State Ionics*, 69, p. 293-305.
24. El Ouatani, L.; Dedryvère, R.; Siret, C.; Biensan, P.; Reynaud, S.; Iratçabal, P.; Gonbeau, D., 2009, The effect of vinylene carbonate additive on surface film formation on both electrodes in li-ion batteries, *J. Electrochem. Soc.*, 156, A103–A113.
25. B. Simon and J.-P. Boeue, 1997, U.S. Pat. 5,626,981.
26. Aurbach, D.; Gamolsky, K.; Markovsky, B.; Gofer, Y.; Schmidt, M.; Heider, U., 2002, On the use of vinylene carbonate (VC) as an additive to electrolyte solutions for li-ion batteries, *Electrochimica Acta*, 47, 9, p. 1423-1439.

27. Takamatsu, D.; Orikasa, Y.; Mori, S.; Nakatsutsumi, T.; Yamamoto, K.; Koyama, Y.; Minato, T.; Hirano, T.; Tanida, H.; Arai, H.; Uchimoto, Y.; Ogumi, Z., 2015, Effect of an electrolyte additive of vinylene carbonate on the electronic structure at the surface of a lithium cobalt oxide electrode under battery operating conditions, *The Journal of Physical Chemistry C*, 119(18), p. 9791-9797.
28. Wiesboeck, R.A., 1972, U.S. Patent 3,654,330.
29. Ding, M. S.; Xu, K.; Jow, T. R., 2000, Liquid-Solid phase diagrams of binary carbonates for lithium batteries. *J. Electrochem. Soc.*, 147, p. 1688-1694
30. Nie, M.; Chalasani, D.; Abraham, D.; Chen, Y.; Bose, A.; Lucht, B., 2013, Lithium-ion battery graphite solid electrolyte interphase revealed by microscopy and spectroscopy, *The Journal of Physical Chemistry C*, 117, p. 1257-1267.
31. Peled, E., 1979, The electrochemical behavior of alkali and alkaline earth metals in nonaqueous battery systems – the solid electrolyte interphase model, *J. Electrochem. Soc.*, 126, p. 2047-2051.
32. Endo, E.; Ata, M.; Tanaka, K.; Sekai, K., 1998, Electron Spin Resonance Study of the Electrochemical Reduction of Electrolyte Solutions for Lithium Secondary Batteries, *J. Electrochem. Soc.*, 145, p. 3757-3764.
33. Besenhard, J. O.; Winter, M.; Yang, J.; Biberacher, W., 1993, Filming mechanism of lithium-carbon anodes in organic and inorganic electrolytes, *J. Power Sources*, 54, p. 228-231.
34. Ohzuku, T.; Iwakoshi, Y.; Sawai, K., 1993, Formation of Lithium-Graphite Intercalation Compounds in Nonaqueous Electrolytes and Their Application as a Negative Electrode for a Lithium Ion (Shuttlecock) Cell, *J. Electrochem. Soc.*, 140, p. 2490-2498.
35. Aurbach, D.; Ein-Eli, Y., 1995, The Study of Li-Graphite Intercalation Processes in Several Electrolyte Systems Using In Situ X-Ray Diffraction, *J. Electrochem. Soc.*, 142, p. 1746-1752.
36. Dahn, J.R., 1991, Phase diagram of Li_xC_6 , *Phys. Rev. B*, 44, p. 9170.
37. Jiang, Z.; Alamgir, M.; Abraham, K. M., 1995, The Electrochemical Intercalation of Li into Graphite in Li/Polymer Electrolyte/Graphite Cells, *J. Electrochem. Soc.*, 142, p. 333-340.
38. Aurbach, D.; Levi, M.D.; Levi, E.; Schechter, A., 1997, Failure and stabilization mechanisms of graphite electrodes, *J. Phys. Chem. B*, 101, p. 2195-2206.
39. Lischka, U.; Wietelmann, U.; Wegner, M., 1999, DE 19829030 C1.

40. Xu, K.; Zhang, S.; Jow, T. R.; Xu, W.; Angell, C. A., 2002, LiBOB as salt for lithium-ion batteries, a possible solution for high temperature operation, *Electrochem. Solid-State Lett.*, 5(1), A26.
41. Xu, K.; Zhang, S.; Poese, B.A.; Jow, T. R., 2002, Lithium Bis(oxalato)borate stabilizes graphite anode in propylene carbonate, *Electrochemical and Solid-State Letters*, 5, A259.
42. Xu, K.; Zhang, S.; Jow, T. R., 2003, Formation of the graphite/electrolyte interface by lithium bis(oxalato)borate, *Electrochem. Solid-State Lett.*, 6, A117.
43. Thinius, S; Islam, M.M.; Heitjans, P; Bredow, T., 2014, Theoretical Study of Li Migration in Lithium–Graphite Intercalation Compounds with Dispersion-Corrected DFT Methods, *Journal of Physical Chemistry C*, 118 (5), p. 2273-2280.
44. Ein-Eli, Y.; Thomas, S.; Koch, V.; Aurbach, D.; Markovsky, B.; Schechter, A., 1996, A Comparative Study of Synthetic Graphite and Li Electrodes in Electrolyte Solutions Based on Ethylene Carbonate-Dimethyl Carbonate Mixtures, *Journal of the Electrochemical Society*, 143 (12), p. 3809-3820.
45. Aurbach, D.; Ein-Eli, Y.; Markovsky, B.; Zaban, A.; Luski, S.; Carmeli, Y.; Yamin, H., 1995, The study of electrolyte solutions based on ethylene and diethyl carbonates for rechargeable Li batteries II. Graphite electrodes, *Journal of The Electrochemical Society*, 142 (9), p. 2882-2890.
46. Aurbach, D.; Zinigrad, E.; Zhongua, L.; Schechter, A.; Moshkovich, M.; Surampudi, S.; Marsh, M., Editors, PV 98-16, p. 95, *The Electrochemical Society Proceedings Series*, Pennington, NJ (1999).
47. Qu, D.; Zheng, D.; Qu, D.; Yang, X.Q.; Yu, X.; Lee, H.S., 2015, Quantitative and qualitative determination of polysulfide species in the electrolyte of a lithium-sulfur battery using HPLC ESI/MS with one-step derivatization, *Adv. Energy Mater.* 5 (2015). doi:10.1002/aenm.201401888.
48. Xia, J.; Petibon, R.; Xiong, D.; Ma, L.; Dahn, J.R., 2016, Enabling linear alkyl carbonate electrolytes for high voltage Li-ion cells, *Journal of Power Sources*, 328, p. 124 -135.
49. Zheng, Z.; Yan, P.; Cao, R.; Xiang, H.; Engelhard, M.H.; Polzin, J.B.; Wang, C.; Zhang, J.G.; Xu, W., 2016, Effects of propylene carbonate content in CsPF₆ -containing electrolytes on the enhanced performances of graphite electrode for lithium-ion batteries, *Applied Material Interfaces*, 8, p. 5715-5722.
50. Smart, M.C.; Lucht, B.L.; Dalavi, S.; Krause, F.C.; Ratnakumar, B.V., 2012, The effect of additives upon the performance of MCMB/LiNi_xCo_{1-x}O₂ Li-Ion cells containing methyl butyrate -based wide operating temperature range electrolytes, *Journal of Electrochemical Society*, 159 (6), A739-A751.

51. Yoshizawa, H. and Tsutomu, O., 2007, An application of lithium cobalt nickel manganese oxide to high-power and high-energy density lithium-ion batteries, *Journal of Power Sources*, 174, p. 813-817.
52. Whittingham, M., 2004, Lithium Batteries and Cathode Materials, *Chem. Rev.*, 104, p. 2471-4301.
53. Zhang, S.S.; Jow, T.R.; Amine, K.; Henriksen, G.L., 2002, LiPF₆ -EC-EMC electrolyte for Li-ion battery, *Journal of Power Sources*, 107, p. 18-23.
54. Zhuang, G.V.; Xu, K.; Yang, H.; Jow, T.R.; Ross, P.N. Jr., 2005, Lithium ethylene dicarbonate identified as the primary product of chemical and electrochemical reduction of EC in 1.2 M LiPF₆/EC:EMC electrolyte, *J Phys. Chem B*. 109 (37), p. 17567-17573.
55. Aiken, C.P.; Xia, J.; Wang, D.Y.; Stevens, D.A.; Trussler, S.; Dahn, J.R., 2014, An apparatus for the study of in situ gas evolution in Li-Ion pouch cells, *Journal of Electrochemical Society*, 161 (10), A1548-A1554.
56. Whitehead, A.H.; Edstrom, K.; Rao, N.; Owen, J.R., 1996, In situ X-ray diffraction studies of a graphite-based Li-ion battery negative electrode, *Journal of Power Sources*, 63, p. 41-45.
57. Cresce, A.; Russell, S.; Baker, D.; Gaskell, K.; Xu, K., 2014, In Situ and Quantitative Characterization of Solid Electrolyte Interphases, *Nano Lett.*, 14, p. 1405-1412.

APPENDICES

Appendix A. -20°C and -30°C discharge capacity for various electrolyte at 5C rate after 100 cycles at 60°C

| Electrolyte names | Solvent ratios | LiPF ₆ | Additives (1 % and 0.5%) | 2 nd -20 ° C (mAh) | 2 nd -30 ° C (mAh) |
|-------------------|--|-------------------|-----------------------------|----------------------------------|----------------------------------|
| 1 | EC/PC/EMC/DMC/DEC 30: 30: 0: 40: 0 | 1.0 M | VC+LiBOB | 0.00 | 0.00 |
| 2 | EC/PC/EMC/DMC/DEC 30: 30: 0: 0: 40 | 1.0 M | VC+LiBOB | 0.09 | 0.03 |
| 3 | EC/PC/EMC/DMC/DEC 20: 30: 10: 0: 40 | 1.0 M | VC+LiBOB | 0.14 | 0.04 |
| 4 | EC/PC/EMC/DMC/DEC 22: 9.9: 48.7: 11: 8.5 | 1.0 M | VC+LiBOB | 0.41 | 0.07 |
| 5 | EC/PC/EMC/DMC/DEC 22: 22.4: 18.7: 28.5: 8.5 | 1.0 M | VC+LiBOB | 0.08 | 0.01 |
| 6 | EC/PC/EMC/DMC/DEC 20: 5: 70: 0: 5 | 1.0 M | VC+LiBOB | 0.17 | 0.03 |
| 7 | EC/PC/EMC/DMC/DEC 27: 9.9: 26.2: 8.5: 28.5 | 1.0 M | VC+LiBOB | 0.14 | 0.02 |
| 8 | EC/PC/EMC/DMC/DEC 20: 5: 70: 5: 0 | 1.0 M | VC+LiBOB | 0.34 | 0.06 |
| 9 | EC/PC/EMC/DMC/DEC 20: 5: 35: 40: 0 | 1.0 M | VC+LiBOB | 0.67 | 0.18 |
| 10 | EC/PC/EMC/DMC/DEC 22: 9.9: 48.7: 8.5: 11 | 1.0 M | VC+LiBOB | 0.29 | 0.06 |
| 14 | EC/PC/EMC/DMC/DEC 13: 3: 0: 30: 25 | 1.0 M | VC+LiBOB | 0.20 | 0.03 |
| 15 | EC/PC/EMC/DMC/DEC 30: 5: 0: 40: 25 | 1.0 M | VC+LiBOB | 0.14 | 0.03 |
| 16 | EC/PC/EMC/DMC/DEC 20: 30: 0: 40: 10 | 1.0 M | VC+LiBOB | 0.08 | 0.01 |
| 17 | EC/PC/EMC/DMC/DEC 20: 5: 0: 35: 40 | 1.0 M | VC+LiBOB | 0.08 | 0.01 |
| 18 | EC/PC/EMC/DMC/DEC 20: 5: 35: 0: 40 | 1.0 M | VC+LiBOB | 0.28 | 0.06 |
| 19 | EC/PC/EMC/DMC/DEC 30: 5: 0: 25: 40 | 1.0 M | VC+LiBOB | 0.26 | 0.05 |
| 20 | EC/PC/EMC/DMC/DEC 30: 5: 25: 0: 40 | 1.0 M | VC+LiBOB | 0.21 | 0.05 |
| 21 | EC/PC/EMC/DMC/DEC 20: 30: 0: 10: 40 | 1.0 M | VC+LiBOB | 0.13 | 0.03 |
| 22 | EC/PC/EMC/DMC/DEC 25: 5: 70: 0: 0 | 1.0 M | VC+LiBOB | 0.33 | 0.06 |
| 23 | EC/PC/EMC/DMC/DEC 30: 5: 65: 0: 0 | 1.0 M | VC+LiBOB | 0.34 | 0.06 |

| | | | | | |
|----|---|-------|----------|------|------|
| 24 | EC/PC/EMC/DMC/DEC 20: 10: 70: 0: 0 | 1.0 M | VC+LiBOB | 0.16 | 0.03 |
| 25 | EC/PC/EMC/DMC/DEC 20: 30: 50: 0: 0 | 1.0 M | VC+LiBOB | 0.19 | 0.05 |
| 26 | EC/PC/EMC/DMC/DEC 30: 30: 40: 0: 0 | 1.0 M | VC+LiBOB | 0.07 | |
| 27 | EC/PC/EMC/DMC/DEC 30: 5: 25: 40: 0 | 1.0 M | VC+LiBOB | 0.18 | 0.03 |
| 28 | EC/PC/EMC/DMC/DEC 20: 30: 10: 40: 0 | 1.0 M | VC+LiBOB | 0.23 | 0.04 |
| 29 | EC/PC/EMC/DMC/DEC 24: 14.8: 27.4: 16.9: 16.9 | 1.0 M | VC+LiBOB | 0.13 | 0.03 |
| 30 | EC/PC/EMC/DMC/DEC 27: 22.4: 13.7: 8.5: 28.5 | 1.0 M | VC+LiBOB | 0.15 | 0.04 |
| 31 | EC/PC/EMC/DMC/DEC 22: 9.9: 13.7: 28.5: 26 | 1.0 M | VC+LiBOB | 0.28 | 0.07 |
| 32 | EC/PC/EMC/DMC/DEC 27: 9.9: 13.7: 28.5: 21 | 1.0 M | VC+LiBOB | 0.24 | 0.05 |
| 33 | EC/PC/EMC/DMC/DEC 22: 22.4: 13.7: 28.5: 13.5 | 1.0 M | VC+LiBOB | 0.17 | 0.03 |
| 34 | EC/PC/EMC/DMC/DEC 27: 22.4: 13.7: 28.5: 8.5 | 1.0 M | VC+LiBOB | 0.07 | 0.01 |
| 35 | EC/PC/EMC/DMC/DEC 22: 9.9: 13.7: 26: 28.5 | 1.0 M | VC+LiBOB | 0.33 | 0.06 |
| 36 | EC/PC/EMC/DMC/DEC 22: 9.9: 31.2: 8.5: 28.5 | 1.0 M | VC+LiBOB | 0.29 | 0.05 |
| 37 | EC/PC/EMC/DMC/DEC 27: 9.9: 13.7: 21: 28.5 | 1.0 M | VC+LiBOB | 0.10 | 0.02 |
| 38 | EC/PC/EMC/DMC/DEC 22: 22.4: 13.7: 13.5: 28.5 | 1.0 M | VC+LiBOB | 0.27 | 0.06 |
| 39 | EC/PC/EMC/DMC/DEC 22: 22.4: 18.7: 8.5: 28.5 | 1.0 M | VC+LiBOB | 0.15 | 0.04 |
| 40 | EC/PC/EMC/DMC/DEC 24.5: 9.9: 48.7: 8.5: 8.5 | 1.0 M | VC+LiBOB | 0.18 | 0.04 |
| 41 | EC/PC/EMC/DMC/DEC 27: 9.9: 46.2: 8.5: 8.5 | 1.0 M | VC+LiBOB | 0.26 | 0.05 |
| 42 | EC/PC/EMC/DMC/DEC 22: 12.4: 48.7: 8.5: 8.5 | 1.0 M | VC+LiBOB | 0.31 | 0.06 |
| 43 | EC/PC/EMC/DMC/DEC 22: 22.4: 38.7: 8.5: 8.5 | 1.0 M | VC+LiBOB | 0.08 | 0.01 |
| 44 | EC/PC/EMC/DMC/DEC 27: 22.4: 33.7: 8.5: 8.5 | 1.0 M | VC+LiBOB | 0.11 | 0.03 |
| 45 | EC/PC/EMC/DMC/DEC 22: 9.9: 31.2: 28.5: 8.5 | 1.0 M | VC+LiBOB | 0.27 | 0.05 |
| 46 | EC/PC/EMC/DMC/DEC 27: 9.9: 26.2: 28.5: 8.5 | 1.0 M | VC+LiBOB | 0.22 | 0.04 |

Appendix B. Elemental concentration on anode for electrolytes with VC and LiBOB additive

| Sample | C1s | | | | O1s | | F1s | | P2p | |
|--------|--------|--------|--------|-------|--------|--------|--------|----------|----------|-------|
| | C-C | C-O | C-H | C=O | C=O | C-O | LiF | LixPOyFz | LixPOyFz | LiPF6 |
| 1 | 15.66% | 16.57% | 8.07% | 6.24% | 12.05% | 23.80% | 5.43% | 9.80% | 1.98% | 0.40% |
| 2 | 13.45% | 9.12% | 8.83% | 2.31% | 21.01% | 3.98% | 20.81% | 16.24% | 3.86% | 0.39% |
| 3 | 13.97% | 14.10% | 3.57% | 1.27% | 14.77% | 10.71% | 19.25% | 17.28% | 4.94% | 0.14% |
| 4 | 12.92% | 9.83% | 4.72% | 3.62% | 20.35% | 6.55% | 18.61% | 18.61% | 4.07% | 0.73% |
| 5 | 17.76% | 10.75% | 7.43% | 3.21% | 14.20% | 11.74% | 17.04% | 14.49% | 3.03% | 0.34% |
| 6 | 24.22% | 9.84% | 8.59% | 2.21% | 15.92% | 12.91% | 13.38% | 9.31% | 2.83% | 0.79% |
| 7 | 17.67% | 10.19% | 14.58% | 3.04% | 17.20% | 13.71% | 6.73% | 12.60% | 4.02% | 0.26% |
| 8 | 17.33% | 10.57% | 4.91% | 3.93% | 16.95% | 12.38% | 14.38% | 14.98% | 4.12% | 0.45% |
| 9 | 7.75% | 14.91% | 7.10% | 1.24% | 15.65% | 0.80% | 33.80% | 15.70% | 2.94% | 0.11% |
| 10 | 14.46% | 7.30% | 4.28% | 4.85% | 15.21% | 14.55% | 15.76% | 17.05% | 5.36% | 1.18% |
| 14 | 18.46% | 17.30% | 5.06% | 3.48% | 14.69% | 15.53% | 9.45% | 11.99% | 3.61% | 0.43% |
| 15 | 22.40% | 12.87% | 9.31% | 2.26% | 16.58% | 13.11% | 7.92% | 11.94% | 3.05% | 0.57% |
| 16 | 21.62% | 11.52% | 7.82% | 2.91% | 21.11% | 11.02% | 6.51% | 12.40% | 4.33% | 0.78% |
| 17 | 14.16% | 14.16% | 6.26% | 4.61% | 19.43% | 5.25% | 15.15% | 14.21% | 6.31% | 0.48% |
| 18 | 13.30% | 6.96% | 6.65% | 1.68% | 13.34% | 16.10% | 18.71% | 18.31% | 4.66% | 0.30% |
| 19 | 19.06% | 18.56% | 10.63% | 4.81% | 13.51% | 14.88% | 8.69% | 7.37% | 2.17% | 0.34% |
| 20 | 11.79% | 10.44% | 6.02% | 1.78% | 15.63% | 14.85% | 14.78% | 18.79% | 5.50% | 0.42% |
| 21 | 15.62% | 14.51% | 5.50% | 6.60% | 22.65% | 2.45% | 13.50% | 13.50% | 5.37% | 0.29% |
| 22 | 16.59% | 11.42% | 4.93% | 4.35% | 15.78% | 13.86% | 16.33% | 12.70% | 3.84% | 0.20% |
| 23 | 16.74% | 6.19% | 7.90% | 2.22% | 16.09% | 13.09% | 16.52% | 16.46% | 4.31% | 0.49% |
| 24 | 27.06% | 16.42% | 17.10% | 3.80% | 20.28% | 3.28% | 6.53% | 3.66% | 1.65% | 0.21% |
| 25 | 19.11% | 15.51% | 5.79% | 4.73% | 16.24% | 16.35% | 8.75% | 10.29% | 3.00% | 0.23% |
| 26 | 15.35% | 14.69% | 10.91% | 1.97% | 18.12% | 13.12% | 12.15% | 7.15% | 5.55% | 0.98% |
| 27 | 11.87% | 6.87% | 4.83% | 4.98% | 21.69% | 7.07% | 16.34% | 20.61% | 5.22% | 0.51% |
| 28 | 17.25% | 6.78% | 3.69% | 4.85% | 18.02% | 11.71% | 15.51% | 17.66% | 3.51% | 1.02% |
| 29 | 19.21% | 16.58% | 3.87% | 3.47% | 13.03% | 10.94% | 6.53% | 22.45% | 3.28% | 0.63% |
| 30 | 16.36% | 5.94% | 4.35% | 1.80% | 17.92% | 13.11% | 18.94% | 16.39% | 5.02% | 0.17% |
| 31 | 15.35% | 9.37% | 9.67% | 6.43% | 17.24% | 17.07% | 2.12% | 16.18% | 6.03% | 0.55% |
| 32 | 33.25% | 17.85% | 11.40% | 4.80% | 15.35% | 7.35% | 5.43% | 3.36% | 1.17% | 0.05% |
| 33 | 44.97% | 11.33% | 10.47% | 6.00% | 10.84% | 11.92% | 4.32% | 0.14% | 0.00% | 0.00% |
| 34 | 20.71% | 18.19% | 5.94% | 2.83% | 24.06% | 6.76% | 5.99% | 10.91% | 4.23% | 0.39% |
| 35 | 24.17% | 7.08% | 6.21% | 3.55% | 16.60% | 17.01% | 10.94% | 11.09% | 2.93% | 0.41% |
| 36 | 18.49% | 9.21% | 10.16% | 5.21% | 16.71% | 16.02% | 7.62% | 13.49% | 2.33% | 0.75% |
| 37 | 34.95% | 15.42% | 9.53% | 6.32% | 9.41% | 12.82% | 5.42% | 4.36% | 1.62% | 0.17% |
| 38 | 15.21% | 8.08% | 9.01% | 2.33% | 18.12% | 11.30% | 12.98% | 18.30% | 4.04% | 0.63% |

| | | | | | | | | | | |
|----|--------|--------|--------|-------|--------|--------|--------|--------|-------|-------|
| 39 | 26.39% | 19.74% | 8.44% | 3.71% | 11.35% | 10.19% | 7.52% | 10.08% | 2.30% | 0.29% |
| 40 | 15.85% | 9.49% | 7.72% | 3.00% | 17.46% | 10.28% | 14.58% | 15.49% | 5.55% | 0.58% |
| 41 | 11.44% | 9.37% | 10.78% | 1.79% | 14.20% | 21.29% | 8.80% | 17.50% | 3.92% | 0.92% |
| 42 | 11.65% | 8.41% | 3.79% | 4.00% | 15.83% | 14.82% | 19.55% | 16.70% | 4.42% | 0.82% |
| 43 | 24.36% | 12.60% | 11.81% | 6.30% | 11.74% | 10.24% | 7.48% | 12.32% | 2.86% | 0.27% |
| 44 | 19.00% | 19.27% | 5.77% | 2.44% | 11.95% | 13.32% | 10.05% | 14.23% | 3.14% | 0.81% |
| 45 | 14.36% | 4.40% | 6.91% | 1.10% | 15.91% | 11.68% | 23.62% | 16.96% | 4.53% | 0.53% |
| 46 | 10.74% | 9.22% | 6.39% | 1.22% | 15.82% | 12.86% | 19.06% | 19.06% | 5.08% | 0.54% |

Appendix C. Cell cycling for electrolyte DOE

| |
|---|
| <i>A. Formation cycles (2 cycles) at room temperature:</i> |
| 1. Cells will be charged by constant current (C/5) until the voltage reaches to 4.1 V (Where, C is cathode capacity). |
| 2. As the 4.1 Volt is reached, the cells will be held constant volt at 4.1 V until the current falls to C/20 (which is 25 % of charging constant current) |
| 3. The cells will be left at rest for 1 minute |
| 4. The cells will be discharged by constant current of C/5 until the voltage reaches to 2.7 V. |
| 5. The cells will be left at rest for 1 minute. |
| 6. Again the cells will be charged as stated in step 1. The steps 2, 3, 4 and 5 are repeated. |
| <i>B. Charge and discharge at room temperature, 25 °C (3 cycles)</i> |
| 1. The cells will be charged by 1C current rate until voltage reaches to 4.1 V |
| 2. As the 4.1 Volt is reached, the cells will be held constant at 4.1 V until the current falls to C/20. |
| 3. The cells will be left at rest for 1 minute |
| 4. The cells will be discharged by constant current of 1C until the voltage reaches to 2.0 V. |
| 5. The cells will be left at rest for 1 minute. |
| 6. The cells will charged again by 1C as step 1. Step 1 to 5 are repeated. |
| <i>C. Charge and discharge at room temperature, 25 °C (1 cycles)</i> |
| 1. The cells will be charged by 1C current rate until voltage reaches to 4.1 V |
| 2. As the 4.1 Volt is reached, the cells will be held constant at 4.1 V until the current falls to C/20. |
| 3. The cells will be left at rest for 1 minute |
| 4. The cells will be discharged by constant current of 5C until the voltage reaches to 2 V. |
| 5. The cells will be left at rest for 1 minute. |
| 6. The cells will charged again by 1C as step 1. Step 1 to 5 are repeated. |
| <i>D. Charge and discharge at low temperature, -20 °C and -30 °C (1 cycle)</i> |
| 1. The cells will be charged by 1C rate at Room Temperature until voltage reaches to 4.1 V |

| | |
|---|--|
| 2. | As the 4.1 Volt is reached, the cells will be held constant at 4.1 V until the current falls to C/20 (which is 5% of charging current) |
| 3. | The cells will be left at -20°C at rest for 2 hour. |
| 4. | The cells will be discharged by 5C rate to 2 V (at -20°C). |
| 5. | The cells will be brought to 25°C and left for 2 hours. |
| 6. | The cells will be charged again by 1 C rate (25°C) as step 1. Step 1 to 5 is repeated. |
| (The same test will also be run at -30°C) | |
| <i>E. Charge and discharge at high temperature, $+60^{\circ}\text{C}$</i> | |
| 1. | The cells will be charged by 1C rate until voltage reaches to 4.1 V. |
| 2. | As the 4.1 Volt is reached, the cells will be held constant at 4.1 V until the current falls to C/20 charging current (i.e. 1 % of 5C) |
| 3. | The cells will be left at rest for 1 minute |
| 4. | The cells will be discharged to 2.7 V by 5C current. |
| 5. | The cells will be left at rest for 1 minute. |
| 6. | The cells will charged again by 1C as step 1. Step 1 to 5 is repeated for 100 cycles |